

ANTHROPOGENIC CONTROLS ON OVERWASH DEPOSITION: EVIDENCE AND  
CONSEQUENCES

Laura J. Rogers

A thesis submitted to the faculty at the University of North Carolina at Chapel Hill in partial fulfillment of the requirements for the degree of Master of Science in the Department of Geological Sciences.

Chapel Hill  
2015

Approved by:

Laura J. Moore

Antonio B. Rodriguez

Tamlin Pavelsky

© 2015  
Laura J. Rogers  
ALL RIGHTS RESERVED

## **ABSTRACT**

Laura J. Rogers: Anthropogenic Controls on Overwash Deposition: Evidence and Consequences  
(Under the direction of Laura J. Moore)

Accelerated sea-level rise and potential future increases in storminess due to climate change will threaten the vitality of barrier islands by lowering their relative elevation and altering overwash frequency. High-density development may further increase island vulnerability by restricting delivery of overwash to the subaerial island. I analyzed pre- and post-Hurricane Sandy (2012) LiDAR surveys of the New Jersey coast to assess human influence. I compared natural environments to two developed environments (commercial and residential) using shore-perpendicular topographic profiles. The volume of overwash delivered to residential and commercial areas is reduced by 40% and 90%, respectively, of that delivered to the natural environment. I use this analysis and an exploratory barrier island evolution model to assess long-term impacts of anthropogenic structures. Simulations suggest natural barrier islands may persist under a range of likely future sea-level rise scenarios (7–13 mm/yr) whereas developed barrier islands will have a long-term tendency toward drowning.

## **ACKNOWLEDGEMENTS**

I would like to express my thanks to my thesis advisor, Dr. Laura J. Moore, my committee, Drs. Tamlin Pavelsky and Antonio B. Rodriguez as well as Drs. Brad Murray and Evan Goldstein for all their support, feedback and engagement throughout this learning process. I must also thank the UNC Geological Sciences' Martin Fund and the NSF Geomorphology and Land Use Program (Grant #EAR 1053151) for their generous funding without which this work would not have been possible.

## TABLE OF CONTENTS

|  |     |
|--|-----|
| LIST OF TABLES.....  | vi  |
| LIST OF FIGURES.....   | vii |
| CHAPTER 1: ANTHROPOGENIC CONTROLS ON OVERWASH DEPOSITION ..... | 1   |
| Introduction.....  | 1   |
| Storm statistics and study area .....                          | 4   |
| Methods and results.....                                       | 5   |
| Overwash analysis .....  | 5   |
| <i>Calculation of overwash extent and volume</i> .....         | 5   |
| <i>Error analysis and field comparisons</i> .....              | 7   |
| <i>Characteristics of overwash deposition</i> .....            | 10  |
| <i>Distribution of overwash</i> .....                          | 11  |
| Long-term impacts on barrier island evolution.....             | 13  |
| Discussion.....  | 14  |
| Conclusion .....   | 18  |
| Tables and Figures.....  | 19  |
| APPENDIX A. INTERPOLATION INDUCED ERROR ANALYSIS.....          | 32  |
| APPENDIX B. FIELD OBSERVATIONS.....                            | 33  |
| REFERENCES .....   | 42  |

## LIST OF TABLES

|   |    |
|---|----|
| Table 1. LiDAR metadata.....  | 19 |
| Table 2. Summary of number and length of transect by environment..... | 19 |
| Table 3. Overwash characteristics by environment.....                 | 19 |
| Table 4. Overwash relationship variables.....                         | 19 |
| Table 5. Input parameters used in Figure 10.....                      | 20 |

## LIST OF FIGURES

|  |    |
|--|----|
| Figure 1. Path of Hurricane Sandy and relative study area locations..... | 21 |
| Figure 2. Study area aerial images.....                                  | 22 |
| Figure 3. Pre and post-storm average elevation profiles.....             | 23 |
| Figure 4. Elevation change models by environment.....                    | 24 |
| Figure 5. Annotated elevation change profile.....                        | 25 |
| Figure 6. Average change profile.....                                    | 26 |
| Figure 7. Overwash thickness comparison.....                             | 27 |
| Figure 8. Linear deposition of overwash.....                             | 28 |
| Figure 9. Overwash deposition distribution.....                          | 29 |
| Figure 10. Barrier island evolution modelling results.....               | 30 |
| Figure 11. Role of pre-storm dune height.....                            | 31 |

## CHAPTER 1: ANTHROPOGENIC CONTROLS ON OVERWASH DEPOSITION

### 1. Introduction

Barrier islands are narrow, low-elevation landforms that are highly sensitive to changes in sea level and storm activity. The population densities of barrier islands along the Atlantic and Gulf coasts of the U.S. are, on average, three times greater than those of coastal states and are increasing [Zhang and Leatherman, 2011]. Additionally, tourism is the largest business sector in the world and coastal tourism, including on barrier islands, is the greatest segment of that global industry [Honey and Krantz, 2007]. Much of the attraction to barrier islands stems from their natural beauty and abundance of recreational opportunities, a consequence of their low elevation, typically only ~2 m above sea level [Psuty, 2002].

The same characteristics that make barrier islands popular places to live and visit also make them especially vulnerable to changing environmental conditions. Conservative estimates predict global sea level will rise between 28 and 61 cm by 2100 [Stocker *et al.*, 2013]. Kopp *et al.* [2014] combine local SLR projections and IPCC representative concentration pathway (RCP) 8.5 projections to suggest a SLR of 0.7 – 1.3 m by the year 2100 in New York City, translating to average rates of 7–13 mm/yr – substantially faster than the current rate of 4 mm/yr based on monthly mean sea level data from 1911 to 2014 (NOAA, 2015). Recent work also suggests climate change will increase the frequency of the most intense hurricanes and tropical storms [e.g., Knutson *et al.*, 2010 and Emanuel, 2013]. The cumulative impact of rising sea level and more frequent, more intense storms will influence the behavior of barrier islands in the future [e.g., Leatherman, 1983; Titus, 1991; Sherwood, 2014; Duran and Moore, 2015].

In recent decades, significant progress has been made in understanding the geological development of barrier islands and the important role of overwash in their evolution. Field-based studies have captured measurements of overwash geometry, volume and spatial configuration [e.g., *Morton and Sallenger, 2003; Donnelly and Sallenger, 2007; Carruthers et al., 2013; Williams, 2015; Shaw et al., 2015; Lazarus and Armstrong, 2015*]. Deposition of overwash sediment can occur as a result of wave run-up exceeding the dune crest (classified as run-up overwash) or as a result of the total water level (tides plus storm surge) exceeding the dune crest (classified as inundation overwash) [*Sallenger, 2000*]. Run-up overwash typically produces overwash fans arising from confined flow, whereas inundation overwash generally results in sheetwash deposits arising from laterally unconfined flow. Back-beach morphology, vegetation and development also affect the shape and characteristics of overwash deposition [*Donnelly et al., 2006*]. *Sallenger et al.* [2001, 2003] and *Stockdon et al.* [2002, 2009] improved upon the accuracy of ground-based methods by introducing the use of LiDAR to resolve beach-change signals. Early work by *White and Wang* [2003] used small-scale LiDAR-derived DEMs to determine spatial patterns of coastal volumetric change. They identified a statistically significant difference in net volumetric change over a four year period in regions of the beach categorized as developed, undeveloped or nourished. Additionally, tools have been developed to model and predict erosion in response to the devastation caused by recent storms such as Hurricanes Katrina and Sandy. These include, but are not limited to, process-based models of waves and sediment transport [e.g., *Roelvink et al., 2009; Palmsten and Holman, 2012*] and statistical Bayesian modeling approaches [e.g., *Plant and Stockdon, 2012*].

Previous studies address the impacts of anthropogenic structures and development on overwash delivery from a purely qualitative perspective, however, and these impacts have yet to

be quantified. Not only is the presence of human development on islands increasingly common, but there is a strong coupling between the socioeconomic value placed on barrier islands and the morphologic evolution of islands themselves [e.g., *Werner and McNamara, 2007; McNamara and Werner, 2008a, 2008b; McNamara and Keeler, 2013; Jin et al., 2013; Lazarus, 2014*]. Anthropogenic influence and associated feedbacks have long been recognized for their impact in other natural systems. For example, anthropogenic modification of river systems interrupts the hydrological cycle and causes magnified flood stages [*Criss and Shock, 2001*] overfishing of the world's fish supply leads to loss of biodiversity [*Jackson et al., 2001*] and increases in wildfire severity have been linked to fire prevention practices, which lead to excess fuel available for burning [*Schoennagel et al., 2004*]. However, our understanding of the feedbacks associated with human alteration of barrier islands is in its early stages.

Because overwash supplies sediment to the subaerial island and is the mechanism by which islands migrate landward and maintain elevation above sea level, loss or reduction of sediment delivery to the island interior may ultimately lead to premature island narrowing and drowning, a phenomenon recognized from numerical models of island behavior [*Magliocca et al., 2011*]. Many barrier island evolution models incorporate overwash flux as an adjustable parameter [e.g., *Wolinsky and Murray, 2009; Lorenzo-Trueba and Ashton, 2014; and Walters et al., 2014*], however overwash flux is poorly constrained (especially as it relates to developed shorelines) and direct measurements of overwash deposition have yet to be used to parameterize overwash flux in models of island evolution.

Here, using LiDAR-based surveys of topography collected before and after Hurricane Sandy along a barrier island in New Jersey, USA, I quantify the impact of anthropogenic structures on the landward extent and volume of overwash deposition relative to a nearby natural

area. I then use these results to parameterize a model of barrier island evolution (from *Lorenzo-Trueba and Ashton*, [2014]) to demonstrate the likely effect of anthropogenically generated differences in overwash delivery on long-term barrier evolution.

## 2. Storm statistics and study area

Classified as a post-tropical cyclone, Hurricane Sandy made landfall northeast of Atlantic City, New Jersey on 29 October 2012 [*Blake et al.*, 2013]. Storm surge coupled with spring tides brought water levels to more than 1 m above average for a full day [NOAA, 2013] and led to record-breaking high water levels throughout New Jersey. Maximum water levels reached 3.5 and 2.0 m MSL at The Battery, NY and Atlantic City, NJ, respectively [NOAA, 2013]. Maximum sustained wind speeds of 130 km/hr with gusts up to 145 km/hr were recorded in New York and New Jersey. The overall minimum central pressure reached 940 mb just hours prior to landfall. Preliminary reports estimate that the storm caused nearly \$50 billion in damage within the U.S. [*Blake et al.*, 2013].

I analyze overwash deposition in four areas within a 60 km alongshore reach north of Sandy's landfall, encompassing three categories of environments: 1) a natural environment, which is relatively undisturbed by human influence; 2) a residential environment, defined as a region of family-size homes built on piling foundations; and 3) a commercial environment, typified by the presence of large commercial buildings built on slab foundations (Figures 1 and 2). A 1.2 km-long alongshore reach within the Edwin B. Forsyth Wildlife Refuge serves as the "natural environment" study site. The "residential environment" consists of two regions for comparison to reduce biases introduced as a result of the relative alongshore location of the environments. The first is within Long Beach Township and the second is 50 km north at Normandy Beach. The boardwalk of Seaside Heights, NJ serves as the "commercial

environment”. The tidal range at all sites is 1.8 m [NOAA, 2013] with prevailing winds from the north-west. Average pre-storm profile elevation ranges from 2.5 m to 4.5 m across the environments (Figure 3) and much of this variation is attributable to differences in development. High water marks left by the storm at the north and south ends of my study area were within 0.25 m, at 2.65 m and 2.40 m (NAVD88; hereafter all elevations are reported relative to datum NAVD88), respectively [McCallum *et al.*, 2013] and maximum wind speeds across the study area were within a 10 km/hr range (Figure 1) [Blake *et al.*, 2013]. The close proximity of my sites, the large size of this “super storm” relative to the length of my study area, and the similarity of both high water mark elevations and wind speeds, allow me to assume that observed differences in overwash extent and volume across the sites are likely to be largely a function of differences in development rather than storm characteristics.

### 3. Methods and results

#### 3.1 Overwash analysis

##### 3.1.1 Calculation of overwash extent and volume

I quantify the impact of anthropogenic development on the delivery of overwash sediment to the island interior by targeting two related parameters: 1) the landward extent of overwash deposition; and 2) the volume of overwash sediment. For the purpose of this study, I define the landward overwash extent as the distance in meters from the pre-storm mean high water (MHW) shoreline to the landward-most reach of overwash deposition (measured perpendicular to the shoreline). Volume of deposition is measured as the total quantity of sediment deposited beyond the pre-storm dune crest. The pre-storm MHW shoreline is defined as the 0.7 m contour line. I use LiDAR first-return surveys collected by the US Geological Survey [Wright *et al.*, 2013] to generate pre- and post-Hurricane Sandy elevation profiles that allow me

to measure variability in three dimensions. Point spacing and system error measurements are summarized in Table 1.

To prepare both pre- and post-storm data sets I use an adaptive TIN densification algorithm within ADPAT 1.0 (USGS developed software [*Zhang and Cui, 2007*]) to remove buildings and vegetation; I use ortho-rectified aerial photos to verify that only bare-earth points are retained. Quick Terrain Modeler grids both data sets to create pre- and post-storm surface models using the dataset point spacing to define the underlying grid spacing and optimize resolution. I difference the two surface models to create a pre- to post-storm elevation change model (Figure 4). Using all three models, I then extract relevant parameters for quantification. The pre-storm MHW shoreline serves as a baseline for measurements collected along cross-shore transects (perpendicular to the shoreline) placed at 10 m alongshore intervals (Figure 5). The number of transects measured and the cross-shore lengths of transects for each environment are summarized in Table 2. Transects reaching into the back-barrier bay are truncated to reflect only sub-aerial data.

To determine the landward extent of overwash deposition at each transect I use the LiDAR-derived elevation-change model in combination with aerial imagery. The landward extent of overwash deposition in the natural environment is easily manually digitized using imagery by visually comparing the pre- and post-storm images to identify the seaward edge of fresh overwash deposits. However, given that manually digitizing from aerial imagery in developed areas is significantly more complex (because limited color contrast makes it difficult to distinguish between overwash sand and pre-existing sand in driveways and yards) I use the overwash extent digitized from imagery in the natural environment to develop a binary change scale (which distinguishes between areas of overwash vs. no overwash) within the LiDAR

elevation-change model. I then apply this binary change scale to the respective LiDAR elevation-change model so that I can clearly see and then manually digitize the landward overwash extent in the residential and commercial areas. A modified use of the Digital Shoreline Analysis System (DSAS [Thieler *et al.*, 2009] calculates the distance from the shoreline to the maximum extent of overwash deposition along each transect. For ease of comparison, I represent overwash extent both dimensionally ( $E_{ow}$ ; absolute extent of overwash in meters) and in a non-dimensionalized form:

$$E_{ow}^* = \frac{E_{ow}}{W_{BI}} \quad \text{Equation (1)}$$

where  $E_{ow}^*$  is non-dimensionalized extent of overwash and  $W_{BI}$  is initial cross-shore width of the barrier island in meters.

To calculate the volume of overwash deposition along each transect, I compute the area under the elevation-change profile and represent these volumes as width-averaged quantities in units of  $\text{m}^3/\text{m}$ . The point at which deposition begins is defined as the location where the elevation change becomes positive; deposition ends at the limit of extent of overwash deposition (Figure 5). I define characteristic overwash deposition geometries for each environment by averaging profiles across each study area (Figure 6).

### 3.1.2 Error analysis and field comparisons

Error in LiDAR data is attributed to a combination of four components: system measurement error, interpolation, horizontal displacement and survey error [Hodgson and Bresnahan, 2004]. Sallenger *et al.* [2003] found they could resolve beach-change signals in LiDAR surveys with a vertical precision of  $\pm 15$  cm. However, when detecting change across temporal scales, relative systematic error (or vertical survey offset) is the most important error to

address [Zhang *et al.*, 2005]. Thus, I compare 20 control points between the pre- and post-storm first-return surveys to determine if relative offset error is a factor. I use building corners for most of my control points, as they are easily identifiable and unlikely to be altered by the storm. Direct comparison of the control points for each survey yields an  $R^2$  correlation of 0.99 with an absolute mean error of less than 5 cm. I therefore consider relative offset error to be negligible.

To quantify errors associated with interpolation I removed 1000 points prior to interpolation for comparison to post-interpolation points. The resulting ~5 cm of vertical error is likely an overestimate as removing 1000 points from the data series increases the distance between points (thereby introducing error). Further error analysis is found in Supplemental Information (SI) A.

To test error estimates and the morphologic change signal, I collected eight slide-hammer Geoprobe cores (in November, 2014) along three transects at designated distances from the MHW shoreline. Cores were collected in my natural area study site where overwash deposits were unlikely to have been disturbed by anthropogenic influences following Hurricane Sandy. Detailed core logs and grain-size analyses are presented in SI B. I measured overwash thickness in the cores as the distance between the ground surface and the first major lithologic contact (typically the contact between medium to coarse sand [overwash] and underlying peat). Comparison of overwash thickness measured in cores versus thicknesses derived from LiDAR observations yields absolute differences ranging from 2 to 40 cm, with an average absolute difference of 18 cm (Figure 7).

The signs of the differences follow expected patterns of morphologic change associated with nearshore beach recovery and landward deflation due to aeolian transport and vegetation loss (Figure 7d) given that I sampled more than two years after Hurricane Sandy. Differences

thus not only include errors arising from the LiDAR analysis but also volumetric changes in overwash deposits that have occurred since deposition. For example, the two cores in which I measured overwash thicknesses of -28 and -24 cm relative to those derived from LiDAR are farthest from the shoreline, have limited vegetation due to overwash burial and are therefore vulnerable to erosion by wind. Additionally, the ground surface in these areas exhibited signs of deflation at the time of core collection; moreover,  $< 1\text{m}^2$  plots of land surrounding proximal vegetation clearly had amassed aeolian sediment. Consequently, significant aeolian reworking had occurred in the exposed, landward-most sections in the two years since Hurricane Sandy. Thus, this process of aeolian reworking and deflation reduced overwash thicknesses measured in these locations relative to the thicknesses measured using LiDAR observations.

I found similar post-storm morphologic changes documented on the seaward side of the island. The two cores I collected closest to the shoreline came from a zone in which recent accretion was apparent, likely via onshore ridge-and-runnel migration of bars. This resulted in field estimates of overwash deposition thickness substantially larger than those derived from the LiDAR analysis. These cores were also collected within a zone where the LiDAR analysis indicates alternation between erosional and accretional areas in close proximity, suggesting that positional error may also be affecting the accuracy with which comparison can be made at these cross-shore locations.

Given the likelihood that accretion and erosion have affected preservation of the overwash signal and that the direction of the differences between remote and field-based measurements are as expected based on likely morphological changes since the storm occurred, I conclude that the LiDAR analysis is likely producing depths that are a reasonable reflection of what would have been observed from field surveys conducted immediately following the storm.

Thus, the average 18 cm difference between the core and LiDAR analysis, if taken to represent the uncertainty in my measurements of overwash deposit thickness from LiDAR observations, is most likely a substantial overestimate of actual uncertainty. Moreover, the average difference is also only 3 cm greater than the 15 cm of error identified as sufficient to resolve changes in morphology by *Sallenger et al.*, [2003]. These findings suggest that the LiDAR analysis is providing a reasonably accurate representation of morphologic change caused by Hurricane Sandy.

### *3.1.3 Characteristics of overwash deposition*

Prior to Hurricane Sandy, the dune crest in the natural area reached an average elevation of 2.5 m and was located approximately 20 m landward of the shoreline. Vegetation consisted of mature dune grasses backed by marsh and previous overwash deposits are clearly visible in pre-storm satellite imagery. To ensure that only the extents of newly deposited overwash fans were analyzed, I completed a pre- and post-storm image comparison.

Dunes in the natural environment were uniformly reduced by 1 m in elevation during Hurricane Sandy. Visual inspection of aerial images indicates deposition consistent with laterally unconfined flow. Landward overwash extent ranged from 188 to 309 meters (average = 252 m) and reached the back-barrier bay in 28% of profiles. The volume deposited ranged from 23 to 125 m<sup>3</sup>/m (Figures 8 and 9, Table 3). Volume of sediment deposited into the back-barrier bay, however, is not captured in measurements, leading to a likely under-prediction of both landward overwash extent and volume of deposition in the natural environment.

In the residential area, pre-storm dune crests averaged 3.5 – 4.5 m in elevation at both sites (not counting breaks in the dunes associated with beach access). Most dunes were reduced by approximately 1 m in elevation during Hurricane Sandy. In both locations, visual inspection

indicates overwash was channelized. These areas of confined flow correspond to locations where overwash penetration was greatest. The average landward overwash extent in the residential environments is 169 meters and volumes range from 2 to 117 m<sup>3</sup>/m (Figures 8 and 9, Table 3).

Likely because a distinct dune line was absent in the commercial area, catastrophic damage to beachfront infrastructure occurred during the storm. The boardwalk is 4.5 m in elevation and 75–100 meters from the shoreline. Regions of confined flow occurred along this section of beach, but were less common than in the residential area (fewer channels per kilometer). The average landward extent of overwash deposition in the commercial environments was 111 meters and overwash volume ranges from 0 to 35 m<sup>3</sup>/m, (Figures 8 and 9, Table 3).

#### *3.1.4 Distribution of overwash*

Where overwash flow was uninhibited by anthropogenic structures (i.e. in the natural environment) no signs of channelized flow were visible, whereas channelized, confined overwash events were prevalent in the residential and commercial environments. Combining measurements from all environments, I compared the landward overwash extent and volume of deposition ( $R^2 = 0.68$ ,  $p < 0.01$ ) (Figure 8a). The resulting statistically significant linear relationship can be described as:

$$V_{ow} = K \times E_{ow} - A \quad \text{Equation (2)}$$

where  $V_{ow}$  is volume of overwash,  $K$  is a coefficient and  $A$  is a constant which accounts for offset between the shoreline and the cross-shore location where overwash begins. When I repeat the same analysis for each environment, the relationships remains linear and statistically significant ( $p < 0.01$  for all environments), but values of  $K$  and  $A$  differ (Figure 8b) (Table 4).

When anthropogenic factors are introduced, both the volume and landward extent of overwash deposition decrease with increasing waterfront development. The average volume of sediment delivered to the residential and commercial environments is reduced to just 60% and 10% of that delivered to the natural environment, respectively. Similarly, the average extent of overwash in the natural environment was more than 2.25 times greater than in the commercial environment. The range of values for both extent and volume (Figure 9) was greatest for the residential environment (shown in both dimensional and non-dimensional terms). Only in the natural environment did overwash extend into the back-barrier bay, (i.e., extent >1 in non-dimensionalized terms, Figure 9c).

I can additionally consider the mass balance for each environment. An important consideration here is that my measurements of the system are not closed because topographic LiDAR data limits the analysis to the subaerial landscape. I calculated the mass balance as the difference between the total volume of sand deposited by overwash and the total volume of subaerial sand eroded, as measured from the shoreline to the bay within an environment. Though sand delivered to, and captured by, the bay in the natural environment could not be accounted for, and although the patterns of deposition were most different between the natural and commercial environments, the mass balance in these two environments was similar: their volumes were within 15% of each other, at an average sand loss of  $5.3 \text{ m}^3/\text{m}$  and  $4.6 \text{ m}^3/\text{m}$  for the natural and commercial environments, respectively. By comparison, the residential area lost an average of  $2.9 \text{ m}^3/\text{m}$  of sand, although this number is likely artificially low because I was unable to account for large amounts of sand eroded from beneath the piling foundations of the many homes located within the zone of erosion (Figure 4), a phenomenon observed in post-storm photographs.

The results of my analysis suggest the following scaling relationships for the volume and extent of overwash deposition as a function of the type of anthropogenic structures present (assuming similar bathymetry and back-barrier elevation), for future use in analytic and exploratory models of barrier island processes:

Equation (3):

|                            | Natural               | Residential                      | Commercial                       |
|----------------------------|-----------------------|----------------------------------|----------------------------------|
| <b>Volume</b>              | $V_{ow,N} = V_{ow,N}$ | $V_{ow,R} = 0.6 \times V_{ow,N}$ | $V_{ow,C} = 0.1 \times V_{ow,N}$ |
| <b>Landward Extent (m)</b> | $E_{ow,N} = E_{ow,N}$ | $E_{ow,R} = 0.7 \times E_{ow,N}$ | $E_{ow,C} = 0.4 \times E_{ow,N}$ |

### 3.2 Long-term impacts on barrier island evolution

I use an exploratory morphodynamic barrier island evolution model, introduced by *Lorenzo-Trueba and Ashton [2014]*, to investigate modes of island behavior under a variety of conditions. This model considers a barrier island cross-section through an idealized geometric configuration and uses a system of equations to determine long-term (decades to centuries to millennia) island tendencies. Three change components (passive flooding due to sea-level rise, shoreface fluxes, and overwash) determine the evolution of the barrier system, which is fully resolved by the shoreline toe, the shoreline, the back-barrier, the barrier height, and the rate of change of the back-barrier height. This system of equations is numerically solved to examine coupled, non-steady-state behaviors that include dynamic equilibrium, height drowning, and width drowning. Height drowning in this model occurs when sediment fluxes due to overwash are insufficient to maintain island elevation relative to rising sea level. Width drowning occurs when sediment flux to the back-barrier is insufficient to maintain island geometry during landward migration.

I use this model to investigate the long-term impact of decreases in overwash delivery on island evolution caused by development. To provide context for considering implications across barrier island systems broadly, I apply generic island characteristics similar to those used by *Lorenzo-Trueba and Ashton* [2014], (Table 5), in conjunction with the empirically derived scaling relationships for overwash flux ( $Q_{ow,max}$ ) I present at the end of Section 3.1.4. *Lorenzo-Trueba and Ashton* [2014] capture impacts of storm frequency and magnitude as well as potential anthropogenic effects in a single term,  $Q_{ow,max}$ , which represents the maximum annual volume of overwash delivered by all storms, and they explore values from 0-100 m<sup>3</sup>/m/yr. For consistency with this previous work, I set  $Q_{ow,max}$  to 30 m<sup>3</sup>/m/yr for the natural environment (set this in context with my calculations, this is equal to 50% of the volume of overwash deposition I calculated for this environment). I then applied Equation 3, yielding scaled  $Q_{ow,max}$  values of 18 and 3 m<sup>3</sup>/m/yr for the residential and commercial environments, respectively. Simulations suggest that decreasing overwash flux to the back-barrier shifts the long-term tendency of the island from dynamic equilibrium to width drowning in the residential environment and to height drowning in the commercial environment at significantly high rates of SLR (> 5 mm/yr) and deeper back-barrier depths (> 5 m) (Figure 10). It should be noted Figure 10c represents a worse-case scenario illustrating that the risk of drowning is greatly increased as the rate of SLR increases and as the depth of the back-barrier bay increases. For comparison, the average depths of Barnegat Bay (NJ, USA), Pamlico Sound (NC, USA) and the Chesapeake Bay (MD/VA, USA) are 1, 2 and 6 meters, respectively [*Miselis et al.*, 2013 and *Urquhart et al.*, 2013].

#### 4. Discussion

The volumes and landward extents of overwash deposition measured in this study are 0–125 m<sup>3</sup>/m and 25–310 m, respectively. These values represent both natural and anthropogenic

environments and fall within the expected range based on previous estimates. *Carruthers et al.* [2013] compile 30 estimates of overwash fan geometric properties from a number of studies and report landward overwash extents of 13–359 m and volumes of 8–190 m<sup>3</sup>/m, respectively. Additionally, the average volume of 62 m<sup>3</sup>/m calculated for my “natural environment” is well in line with that estimated for overwash associated with the Hurricane of 1938 on Long Island, NY of ~54-80 m<sup>3</sup>/m [*Redfield and Miller, 1957*], an environment broadly similar to that studied here.

My results extend previous work on overwash by demonstrating a linear relationship between overwash extent and volume (Figure 8). Furthermore, my findings demonstrate that as the landward extent of overwash deposition increases, the relationship with overwash volume becomes less tightly constrained and the range of overwash volumes for any given landward overwash extent increases. This latter phenomena is likely the result of progressive increases in lateral spreading and infiltration which occur as the landward overwash extent increases, a process described in detail by *Donnelly et al.*, [2009].

Similar to previous studies, which cite beach access points and roads as likely conduits for channelized overwash deposition [e.g., *Hall and Halsey, 1991; Nordstrom, 1994; Houser, 2013*], I find a greater frequency of channelized deposits in the residential and commercial environments relative to the natural environment. Analysis of aerial imagery suggests that locations of channelized flow within the developed environments in my study correspond to roads and beach access points. This indicates that infrastructure (i.e., roads, parking lots, etc.) and building placement can control overwash deposition. Further, I found pre-storm dune height to be weakly correlated with overwash extent and volume ( $R^2 = 0.38$  and  $R^2 = 0.30$ , respectively) yet statistically significant ( $p < 0.01$ ) (Figure 11). Although a weak, yet statistically significant relationship exists between pre-storm dune height and overwash

deposition, dune height is not strongly predictive of overwash deposition in this case, likely because dune erosion was so extreme as a result of the high intensity and long duration of Hurricane Sandy. This lack of correlation with pre-existing beach morphology further signifies the role of anthropogenic influence on deposition of overwash.

The volume of overwash deposition varied according to the type of environment, decreasing to 60% and 10% of that delivered to the natural area in the residential and commercial environments, respectively. Because much of the deposition occurring in the developed environments amassed in roads as channelized deposition, the relative volumes measured in this study should be considered upper bounds on deposition; humans will undoubtedly move sand back to the beach (i.e., bulldoze to clear roads) during clean-up (in my study I used post-storm surveys collected prior to clean-up). Additionally, sand delivered to the back-barrier bay in the natural environment was not captured due to limitations of topographic (in contrast to bathymetric) LiDAR. These factors imply the spread between the amount of overwash sediment delivered to the natural and developed environments is likely even greater than my calculations suggest.

The most dramatic reduction in overwash occurred in the commercial area where, despite the record high water levels produced by Hurricane Sandy, overwash extent was limited to the area seaward of the boardwalk along nearly 50% of transects. This suggests that, in the presence of buildings having a substantial alongshore extent, even major storms are unable to supply overwash sediment to the island interior. From this we can infer that smaller, more frequent storms are also unable to supply sediment to the interior of the island, thereby implying that development effectively filters high-frequency events.

Previous modeling studies [*McNamara and Werner, 2008a; Magliocca et al., 2011*] warn of the long-term consequences of filtering high-frequency overwash events arising from protection of infrastructure in the short-term (for example, by building a seawall or large artificial dunes), which may lead to barrier narrowing and drowning. Similar filtering of high-frequency events by anthropogenic manipulation is a recognized phenomenon with major consequences in other geomorphic systems such as major rivers and forested areas [e.g., *Criss and Shock, 2001; Schoennagel et al., 2004*]. Ultimately, the filtering of smaller events has historically led to more extreme, more costly events as demonstrated by river discharge management, wildfire prevention and as predicted in coastal economic models by *McNamara and Werner [2008a]*.

My observational and modeling results suggest that increases in the density and extent of development along barrier island coastlines will reduce overwash delivery, maintaining low barrier islands even as sea levels rise, ultimately leading to increases in damage to infrastructure and higher costs of recovery following large, overwash-producing events. My model results also highlight the potentially catastrophic consequences of high-frequency filtering as it relates to the persistence of barrier islands—they suggest that developed barrier islands will tend toward drowning in the long term under anticipated accelerated SLR, whereas natural barriers will be more likely to persist by means of landward migration via frequent overwash. Thus, we can likely expect filtering of high-frequency—and partial filtering of the low-frequency—delivery of overwash to ultimately impact not only barrier island evolution, but also coastal management decision-making and policy (e.g., cost of insurance). Further work exploring the effects of back-barrier bay depth (i.e., accommodation), interactions between barriers and back-barrier marshes [*Walters et al., 2014*], and complex barrier – inlet – back-barrier dynamics [*FitzGerald et al.,*

2008] on island response to decreased overwash delivery, as well as the potentially compounding effects of offshore bars and beach slope on alongshore variation in water level [*Cohn et al.*, 2014] would potentially broaden the results found here.

## 5. Conclusions

I analyzed two key parameters – volume of overwash deposition and landward extent of overwash deposition – to quantify anthropogenic controls on the delivery of overwash sediment. By categorizing the section of the New Jersey shoreline immediately north of where Hurricane Sandy made landfall into three distinct environments – natural, residential and commercial – I was able to directly compare overwash characteristics under similar storm and initial morphologic conditions. The volume of deposition in the residential and commercial environments scaled to 60% and 10%, respectively, of the volume deposited in the natural environment volume. This translates into a reduction of overwash delivery by 40% in the residential areas and 90% in the commercial area. The landward extent of overwash was also substantially reduced with increasing shoreline development: in the commercial area, overwash was completely obstructed along 50% of the alongshore reach. This finding suggests that large anthropogenic structures are highly effective at filtering overwash events.

The scaling relationships offered here provide a solid empirical foundation that can be used to parameterize overwash delivery when modeling barrier island evolution in the presence of infrastructure. Model results suggest that anthropogenic reductions in the flux of overwash sediment reaching island interiors may ultimately lead to island drowning. Although Hurricane Sandy was an extreme, low frequency event, it serves as a good example of the depositional impacts that can be expected in the future with rising sea levels and the increased frequency of more intense storms.

## 6. Tables and Figures

**Table 1.** LiDAR metadata

| Location:        | Storm:                   | Collected by:  | Collection Date: | Vertical/Horizontal Accuracy: | Point Spacing: |
|------------------|--------------------------|----------------|------------------|-------------------------------|----------------|
| Ocean County, NJ | Hurricane Sandy – Before | USGS – EAARL-B | 26 Oct 12        | 20 cm/1 m                     | 0.5 – 1.6m     |
|                  | Hurricane Sandy – After  | USGS – EAARL-B | 01-05 Nov 12     | 20 cm/1 m                     | 0.5 – 1.6m     |

**Table 2.** Summary of number and length of transect by environment

| Location (Environment)        | Number of Transects | Maximum Length (m) |
|-------------------------------|---------------------|--------------------|
| Edwin B. Forsythe (Natural)   | 122                 | 325                |
| Long Beach Twp. (Residential) | 132                 | 425                |
| Normandy Beach (Residential)  | 99                  | 425                |
| Seaside Heights (Commercial)  | 92                  | 400                |

**Table 3.** Overwash characteristics by environment

| Environment | # of Transects | $E_{OW}$ Range (m) | Avg. $E_{OW}$ (m) | Avg. $E_{OW}^*$ | $V_{OW}$ Range (m <sup>3</sup> /m) | Avg. $V_{OW}$ (m <sup>3</sup> /m) |
|-------------|----------------|--------------------|-------------------|-----------------|------------------------------------|-----------------------------------|
| Natural     | 122            | 188 – 309          | 252.2             | 0.85            | 23.3 – 125.7                       | 62.2                              |
| Residential | 231            | 103 – 271          | 169.0             | 0.47            | 2.1 – 116.7                        | 38.1                              |
| Commercial  | 92             | 25 – 203           | 108.1             | 0.27            | 0 – 35.1                           | 7.7                               |

**Table 4.** Overwash relationship variables<sup>a</sup>

| Environment | $K$  | $A$ |
|-------------|------|-----|
| Combined    | 0.36 | -26 |
| Natural     | 0.40 | -39 |
| Residential | 0.39 | -27 |
| Commercial  | 0.14 | -8  |

<sup>a</sup> $K$  – relationship coefficient,  $A$  – shoreline to overwash offset constant

**Table 5.** Input parameters used in Figure 10

| Parameter                    | Symbol        | Units                          | Value   |
|------------------------------|---------------|--------------------------------|---------|
| Shoreface Response Rate      | $K$           | $\text{m}^3/\text{m}/\text{y}$ | 10,000  |
| Equilibrium Shoreface Slope  | $\alpha$      | -                              | 0.02    |
| Shoreface Toe Depth          | $D_t$         | m                              | 10      |
| Equilibrium Island Width     | $W$           | m                              | 300     |
| Equilibrium Island Height    | $H$           | m                              | 2       |
| Back Barrier Bay Depth       | $D_b$         | m                              | 2, 5, 9 |
| Sea Level Rise               | $z$           | mm/yr                          | 0 – 15  |
| Max. Overwash Flux (Natural) | $Q_{ow, max}$ | $\text{m}^3/\text{m}/\text{y}$ | 30      |
| Max. Overwash Flux (Res.)    | $Q_{ow, max}$ | $\text{m}^3/\text{m}/\text{y}$ | 18      |
| Max. Overwash Flux (Comm.)   | $Q_{ow, max}$ | $\text{m}^3/\text{m}/\text{y}$ | 3       |

Figure 1

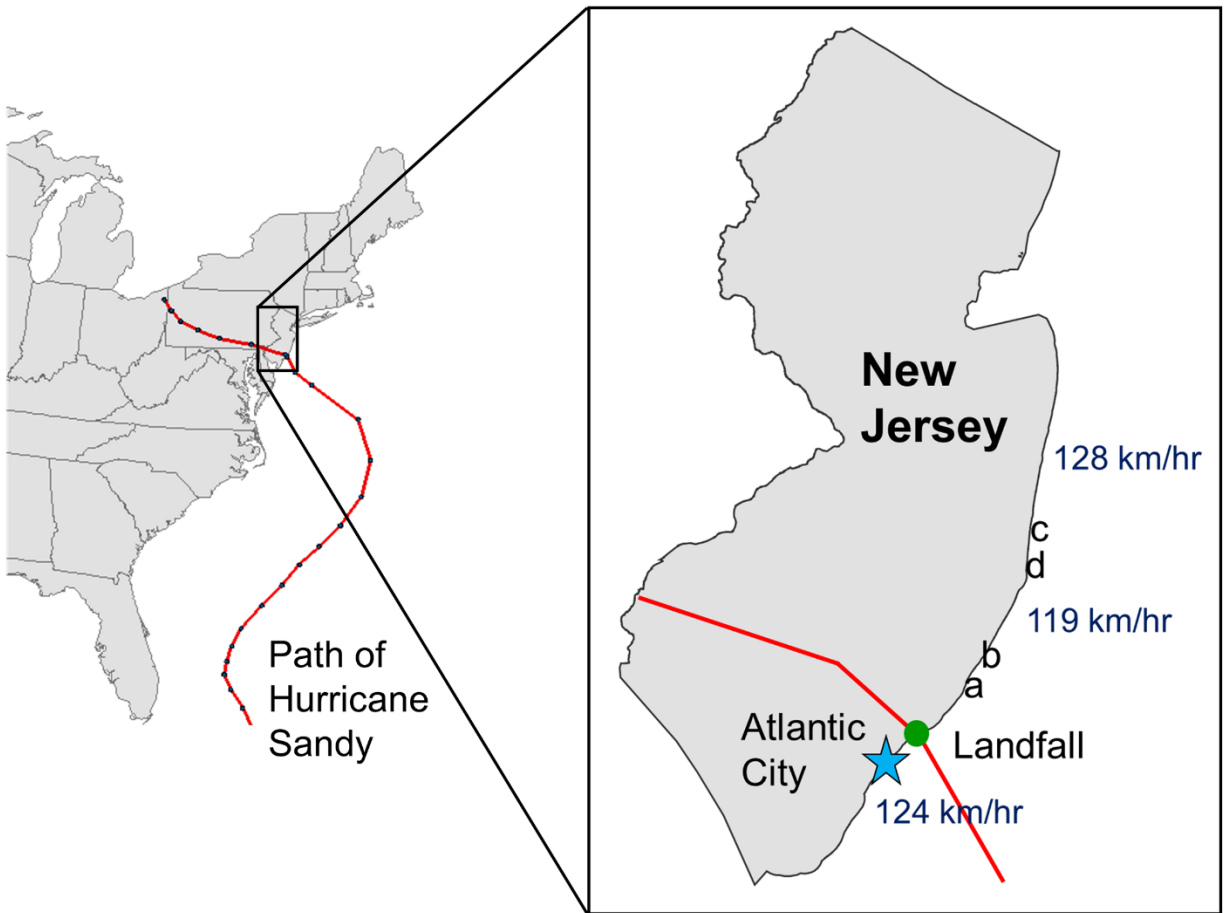


Figure 1. Path of Hurricane Sandy and location of study sites relative to the storm's landfall. Maximum wind speeds (km/hr) along the coast are depicted in dark blue. Post-Sandy images shown in Figure 2.

Figure 2

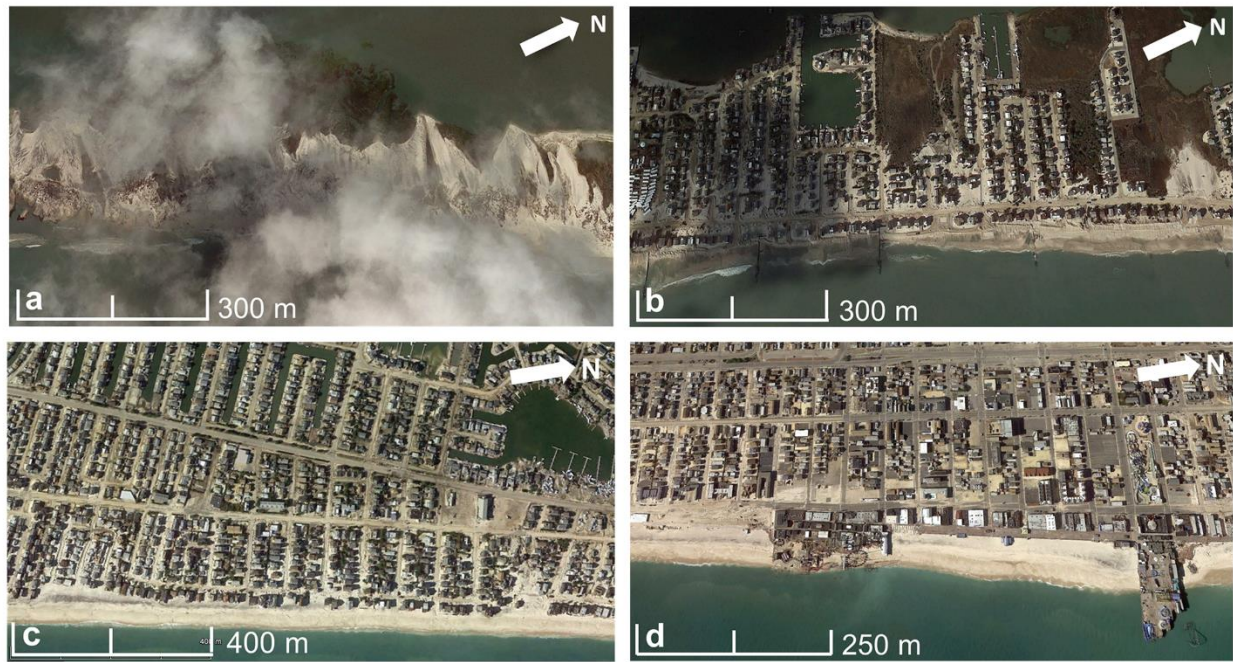


Figure 2. Post Hurricane Sandy aerial images of each study site (refer to Figure 1 for relative locations) (a) the natural area site at Holgate (b) residential site in Long Beach Township (c) residential site at Normandy Beach, and (d) commercial site at the Seaside Heights boardwalk. Imagery Source: Google Earth, 3 Nov 2012.

Figure 3

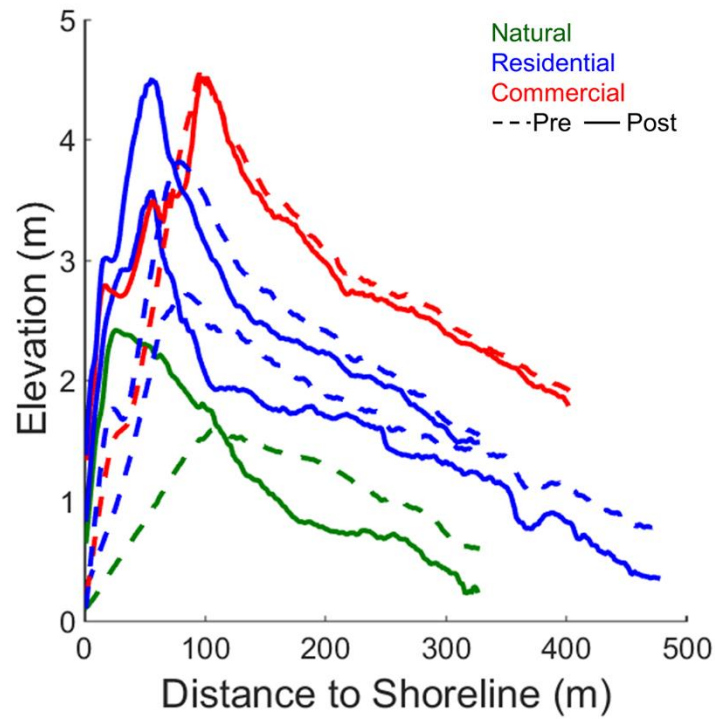


Figure 3. Average pre- and post-storm elevation profiles (based on 90-130 profiles for each area, see Table 2) for the specified environment showing the degree of change in erosional patterns shoreward of the dune crest as well as change in dune elevation and deposition thickness beyond the dune.

Figure 4

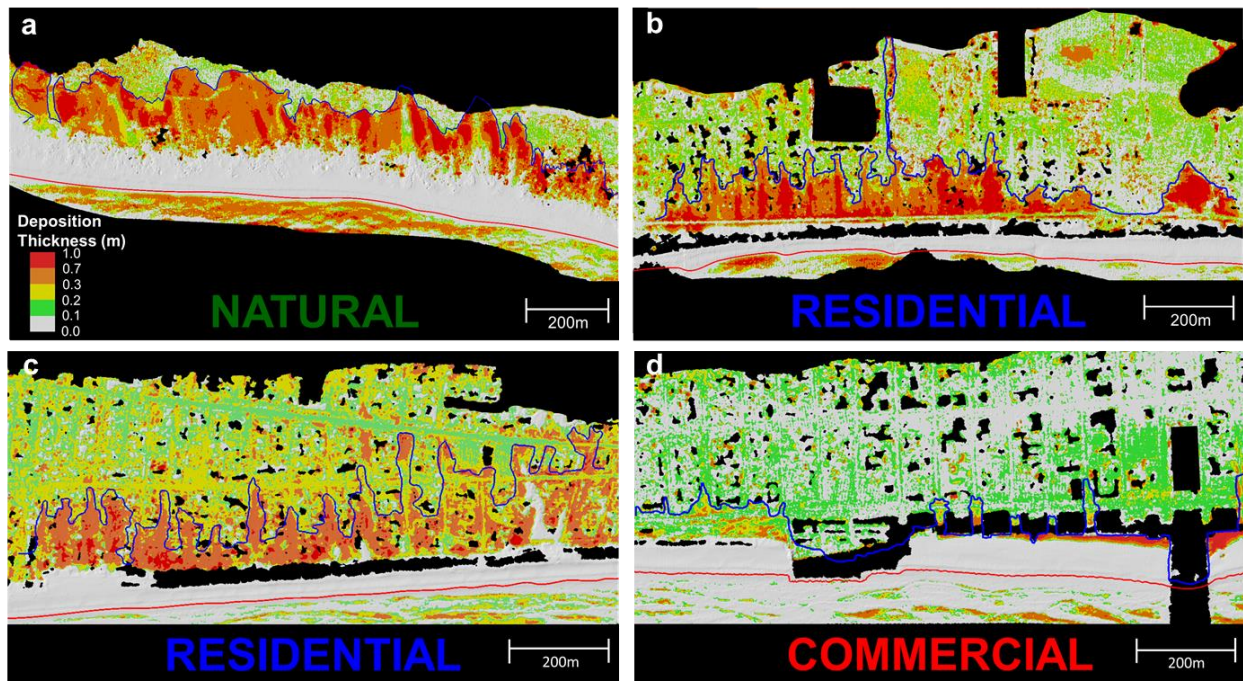


Figure 4. Elevation change models depicting the thickness of sediment deposition and the digitized extent of overwash shown in blue. The mean high water shoreline is shown in red. (a) Natural environment, (b) and (c) residential environments, and (d) the commercial environment.

Figure 5

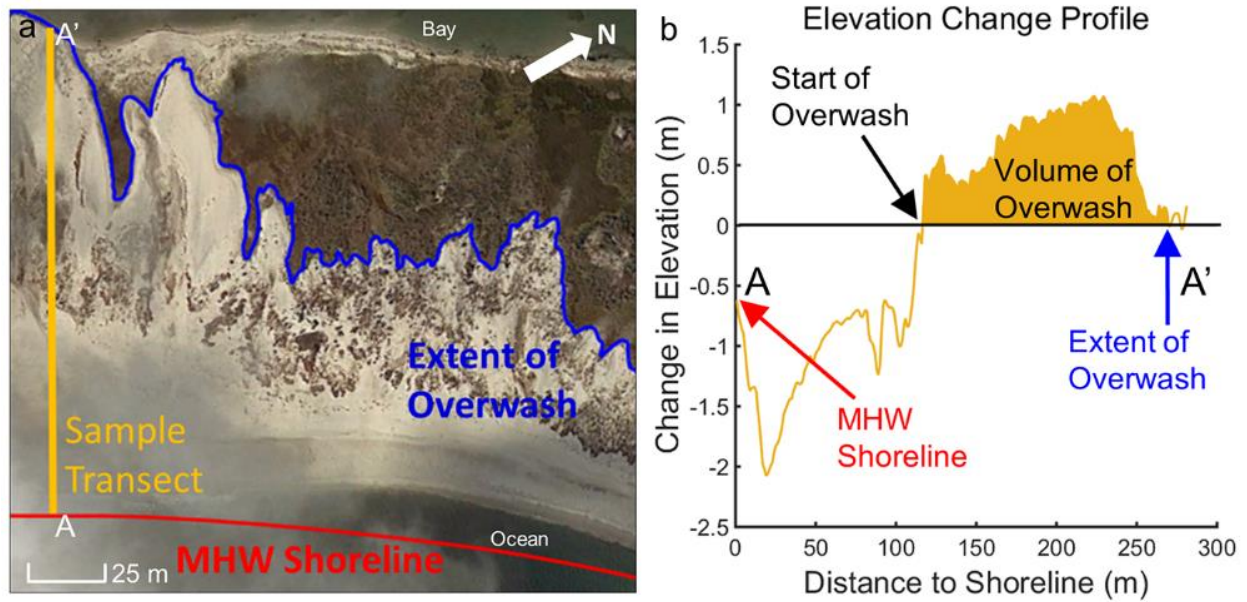


Figure 5. (a) Depiction of the pre-storm mean high water (MHW) shoreline, post-Sandy overwash extent and sample cross-shore transect. (b) Annotated change profile along a cross-shore transect from A to A' (location shown in a) measured from the shoreline showing the start, extent and volume of an overwash deposit.

Figure 6

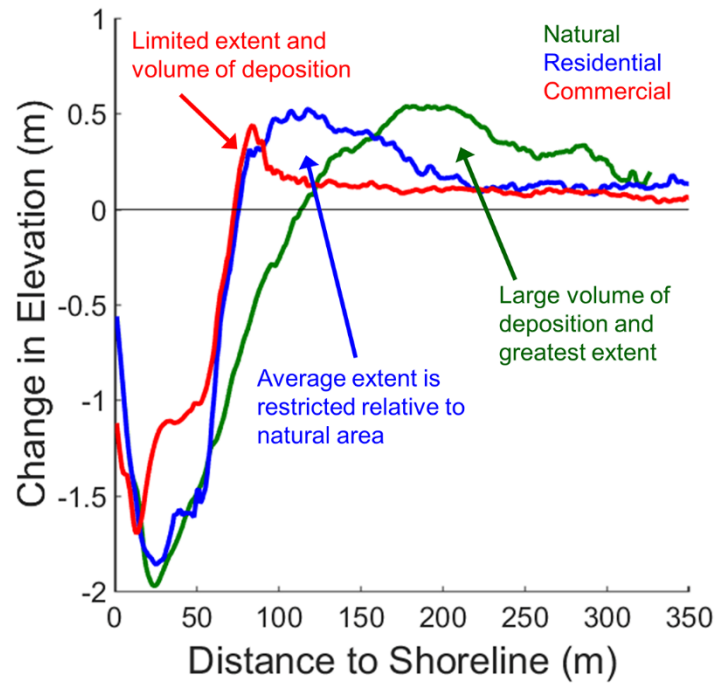


Figure 6. Average change profiles for each environment show patterns of erosion and overwash distribution. In the natural environment, erosion extends farther landward, but overwash deposits are greater in volume and landward extent relative to developed areas.

Figure 7

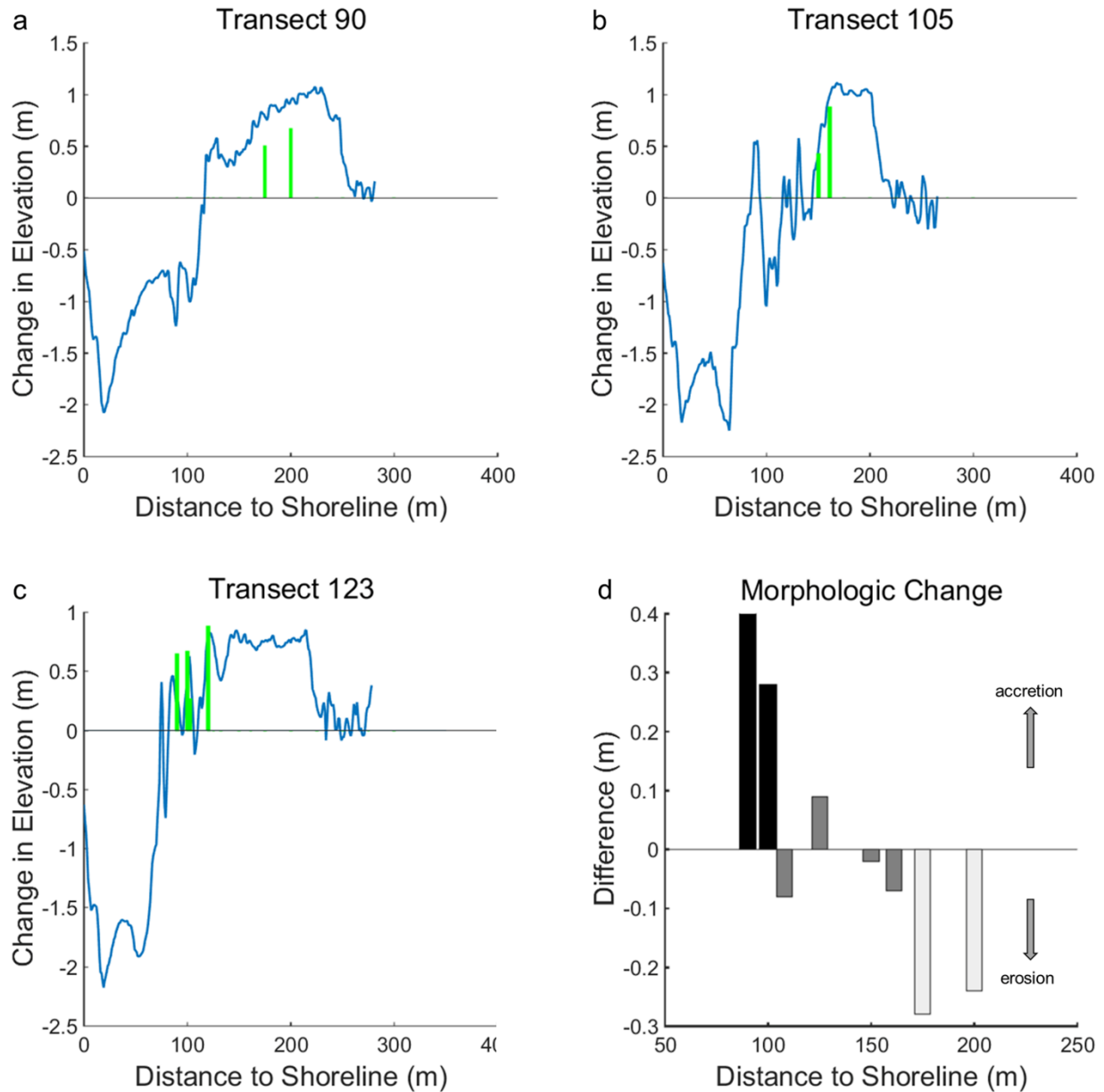


Figure 7. (a-c) LiDAR-derived elevation change profiles (blue lines) compared to overwash thicknesses identified in sediment cores (green lines). This comparison yields absolute differences ranging from 2 to 40 cm, with an average absolute difference of 18 cm. (d) The difference between LiDAR-derived overwash thickness and overwash thickness derived from cores illustrating morphologic change occurring between time of LiDAR surveys and sediment core collection – accretion nearest the shoreline and deflation toward the back-barrier bay.

Figure 8

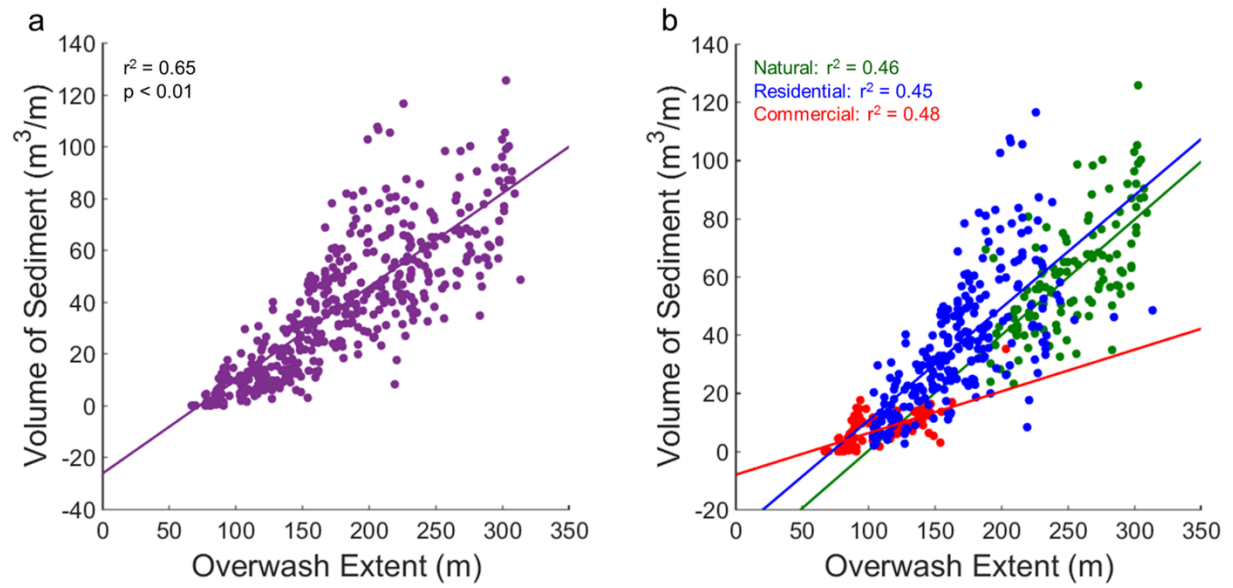


Figure 8. (a) The linear dependence of overwash volume on overwash extent, accounting for the offset between the mean high water shoreline and the cross-shore location where overwash begins. (b) Separating by environment, the relationship remains linear.

Figure 9

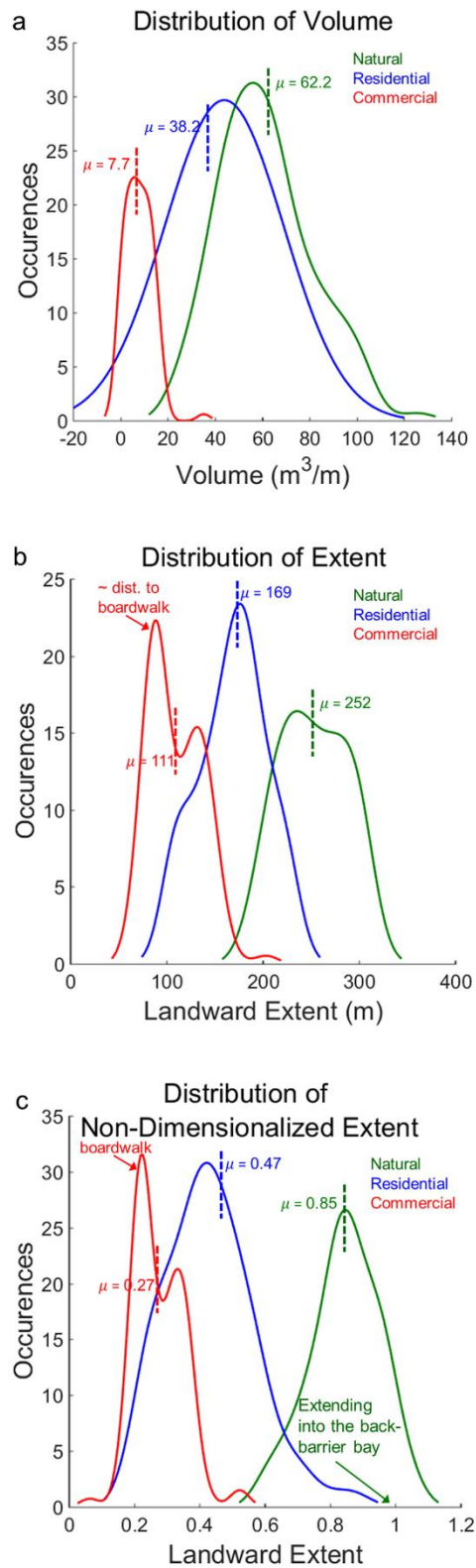


Figure 9. Distribution of (a) overwash volume (b) landward extent of overwash and (c) non-dimensionalized extent of overwash. The natural environment allows the greatest volume and extent of overwash deposition while the commercial environment is most restrictive, reducing the volume of overwash delivered to the residential and commercial environments by 40% and 90%, respectively.

Figure 10

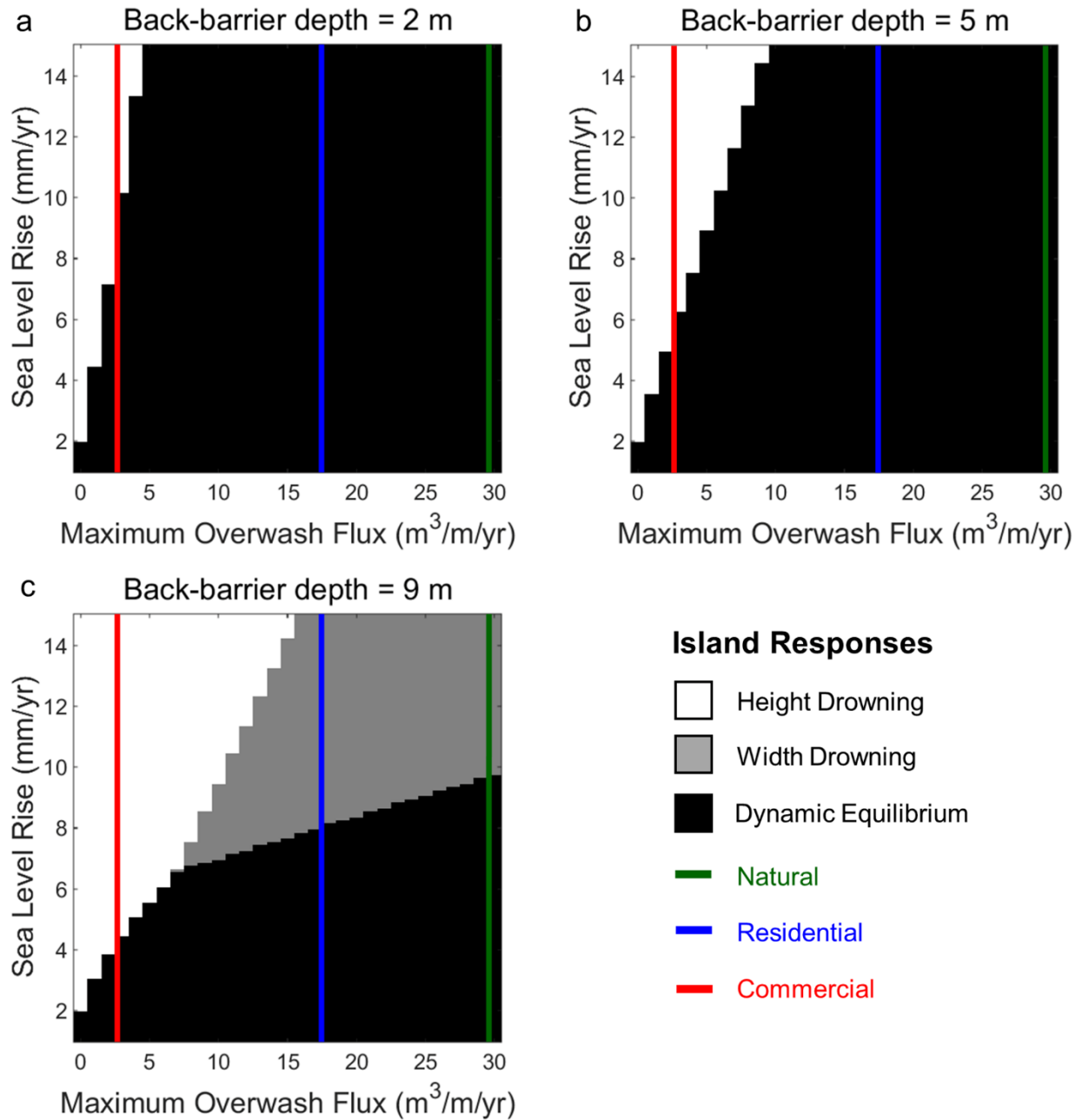


Figure 10. Phase diagrams illustrating the impact of anthropogenic development on barrier island evolution for different rates of sea-level rise, maximum overwash flux and back-barrier depths of (a) 2m, (b) 5m, and (c) 9m. Red and blue lines denote maximum overwash flux ( $Q_{ow,max}$ ) for commercial and residential environments, respectively, scaled relative to a natural environment  $Q_{ow,max}$  of  $30 \text{ m}^3/\text{m}/\text{yr}$  according to relationships presented in Section 3.1.4.

Figure 11

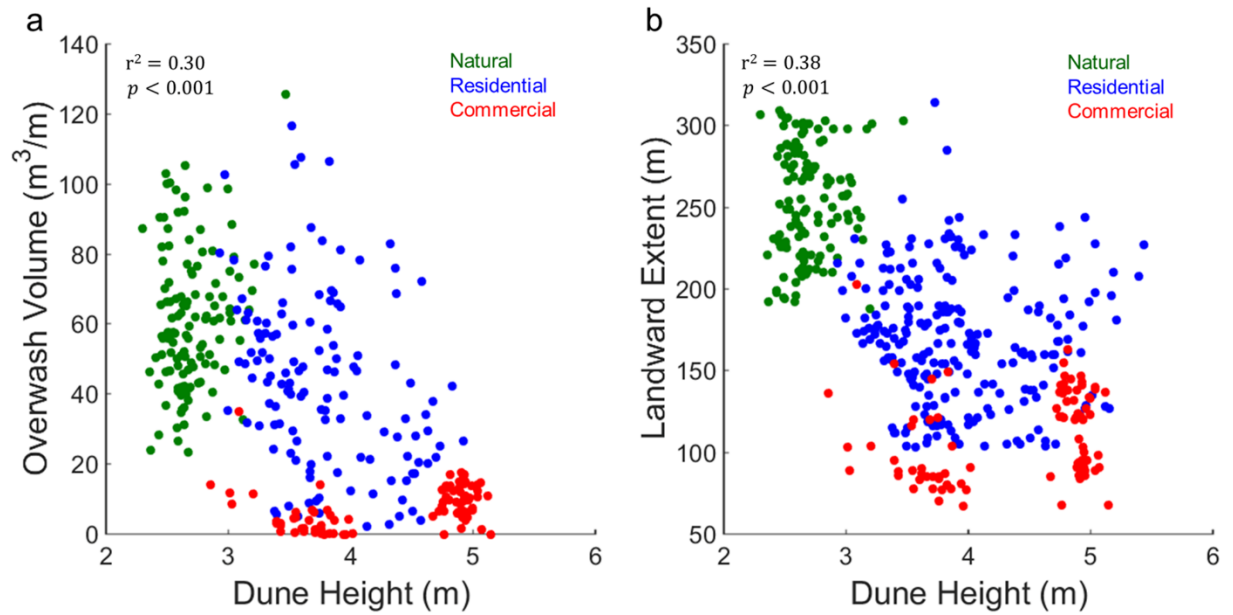


Figure 11. Role of pre-storm dune height on overshash deposition volume and landward extent of overshash. Each data point represents one transect within the designated environment. Pre-storm dune height and (a) overwash volume and (b) overwash extent are both negatively, but weakly, correlated.

## **APPENDIX A: INTERPOLATION INDUCED ERROR ANALYSIS**

Triangulation methods are sensitive to the position of data points and the removal of points (as described in Section 3.1.2). Because the removal of points to assess accuracy results in increases in local point spacing, point removal to quantify induced error due to triangulation likely provides an overestimate of actual error. QT Modeler's RMSE calculation provide an additional measure of error introduced by interpolation. After the gridding process is complete, QT Modeler calculates the RMSE of each 1 m grid square by comparing the original point cloud to the gridded surface without the actual removal of points. This resulted in a similar, yet smaller, induced error with a maximum RMSE of 0.054 m.

## **APPENDIX B. FIELD OBSERVATIONS**

In order to compare the remotely-sensed LiDAR observations analyzed for this study with field observations, I collected cores and grab samples of surficial sediment from the Edwin B. Forsythe Wildlife Refuge, Holgate, New Jersey. Field sampling was done November 15-16, 2014, approximately two years after the LiDAR survey was completed November 1-5, 2012.

The tidal range in this area is 1.8 m [NOAA, 2012] with prevailing winds from the northwest. Prior to the storm, dunes in this area averaged 2.5 m in elevation, located, on average, 20 m from the shoreline. Vegetation consisted of mature dune grasses backed by marsh. Hurricane Sandy delivered large amounts of overwash to the region. The original dune line was reduced by 1 m or more and vegetation was buried or removed by the storm.

Within the area of interest, I selected eight cross-shore transects for sampling (Figure B.1). I collected nine slide-hammer Geoprobe sediment cores samples (Figure B.2), at designated locations. Sample locations were selected based on ground-penetrating radar (GPR) profiles collected concurrently using a Mala ProX with both 250 MHz and 500 MHz antennas. Cores were collected in 6 cm diameter polycarbonate liners within a stainless steel core barrel (Figure B.2). Cores ranged from 65 cm to 175 cm in depth. Additionally, hand auger cores were collected at 25 m intervals along each of the eight transects with the intention to visually identify overwash layers in the field.

Cores were opened, described, photographed, and sampled at the University of North Carolina, Chapel Hill. Three representative cores are shown here (Figures B.3 – B.5). Based on visual inspection and with the intention to compare down-core changes in grain size with the extent of overwash, I selected three cores for detailed grain size analysis: BH123-2-2, BH105-5 and BH90-7, which are 90 m, 150 m and 200 m from the pre-storm MHW shoreline, respectively

(Figure B.6). I collected samples for grain size analysis at 15 cm intervals. Each sample was exposed to 600<sup>0</sup> C temperatures to remove organics, then analyzed using a Beckman Coulter LS 3 Series Laser Diffraction Particle Size Analyzer. The Wentworth scale was used to define general grain size classes. Given the large sampling interval of 15 cm, the overwash depths identified visually as described in Section 3.1.2 are generally comparable to overwash depths identified using grain size analysis.

Comparison of overwash depths measured using LiDAR data with overwash depths measured in the sediment cores reveals general similarities but indicates that (as expected) changes have occurred due to natural beach processes in the intervening two years. I consider all cores in my comparison, except for core BH-105-4-2, which was accidentally collected below the depth of the base of the overwash signal I was attempting to capture (the overwash layer was estimated, based on LiDAR analysis, to begin at a depth of 49 cm, but I augered to a depth of 78 cm before collecting my core sample). The resulting absolute range of difference between the LiDAR analysis and the overwash thickness identified in my cores was 2 to 40 cm with an average absolute difference of 18 cm (Table B1, Figure 5). As explained in Section 3.2, the sign of the differences is reflective of the patterns of morphological diagenesis associated with recovery (close to shore) and deflation (toward the back of the island) in the two years between the storm and field sampling.

**Table B.1.** Sediment core locations and overwash depth comparisons

| Core    | Dist. to<br>Shore (m) | Northing   | Easting     | Overwash<br>Depth in<br>Core (cm) | Overwash<br>Depth from<br>LiDAR (cm) | Diff.<br>(cm) |
|---------|-----------------------|------------|-------------|-----------------------------------|--------------------------------------|---------------|
| 90-6    | 175                   | 4375769.32 | 562732.7499 | 50                                | 78                                   | -28           |
| 90-7    | 200                   | 4375779.85 | 562714.5323 | 67                                | 91                                   | -24           |
| 105-4-2 | 133                   | 4375635.87 | 562667.5412 | 126                               | 49                                   | -             |
| 105-5   | 150                   | 4375640.61 | 562661.2974 | 43                                | 45                                   | -2            |
| 105-5-2 | 161                   | 4375649.33 | 562653.2076 | 88                                | 95                                   | -7            |
| 123-2-2 | 90                    | 4375468.65 | 562592.7106 | 65                                | 25                                   | +40           |
| 123-3   | 100                   | 4375474.94 | 562585.7235 | 67                                | 49                                   | +28           |
| 123-3-2 | 103                   | 4375476.04 | 562583.4492 | 27                                | 35                                   | -8            |
| 123-3-3 | 125                   | 4375483.75 | 562574.1972 | 88                                | 79                                   | +9            |

Figure B.1

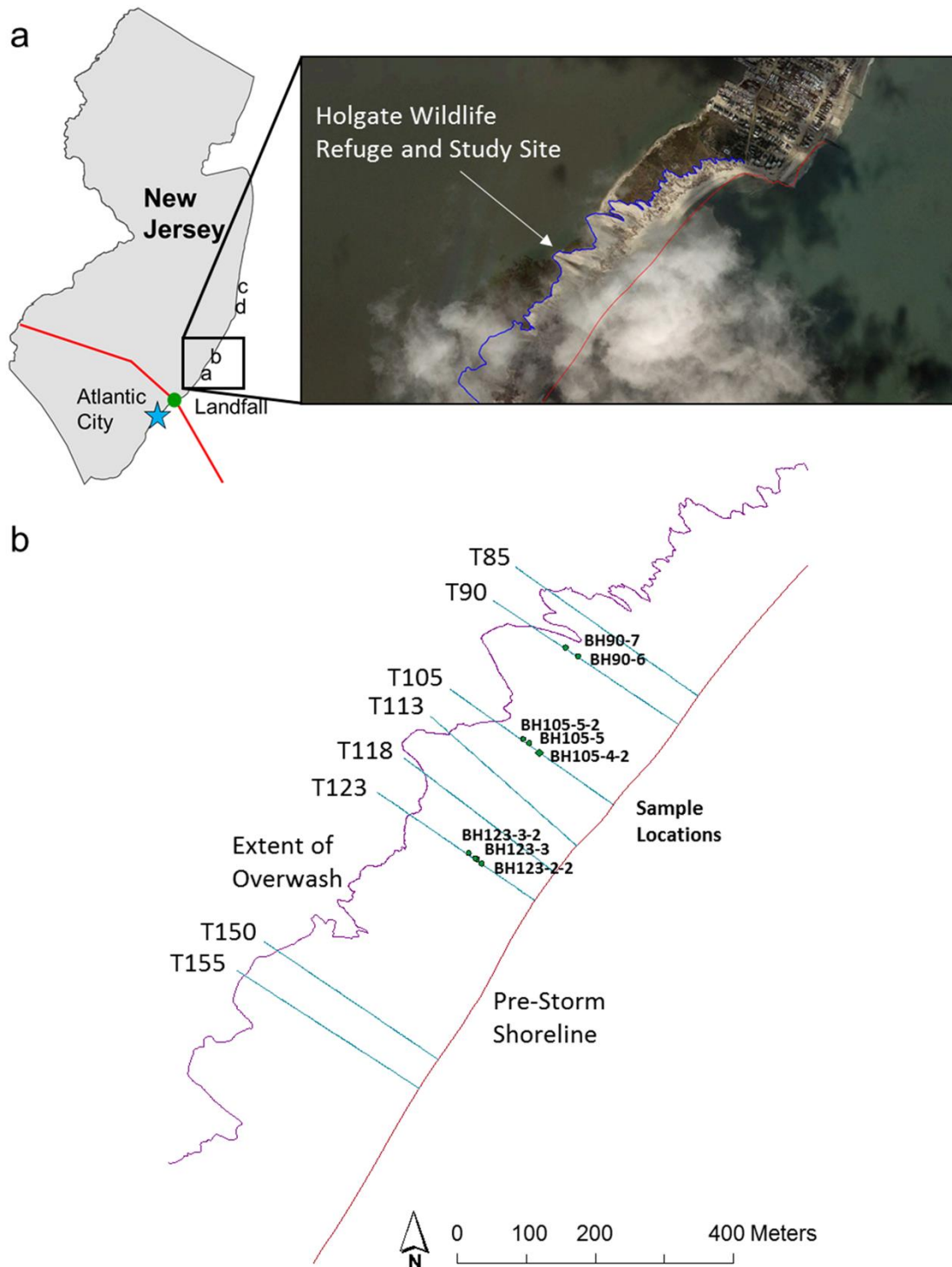


Figure B.1. (a) Map of the study area relative to the path of the storm. The Edwin B. Forsythe Wildlife Refuge is located north of Atlantic City, NJ and is the location of my “natural” analysis site. (b) Location and naming of eight transects and sediment core locations.

Figure B.2



Figure B.2. Photos from the study site. (a) Slide-hammer Geoprobe core collection tools and methods. (b) and (c) Photos along Transect 90 looking west toward Barnegat Bay depicting vertical accretion occurring in the presence of vegetation and deflation occurring in the absence of vegetation.

Figure B.3

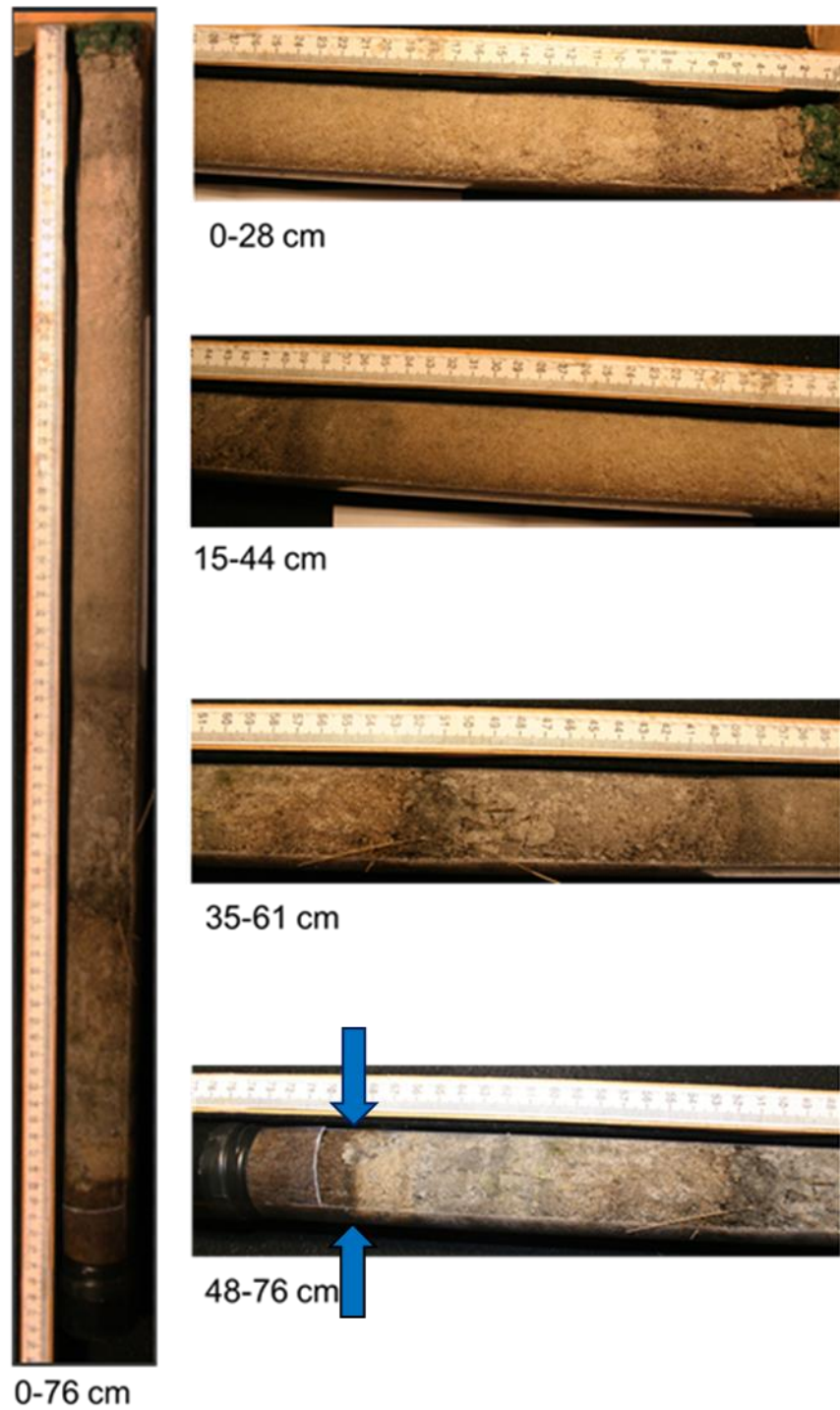


Figure B.3. Core BH-90-7 (200 m from the shoreline). Overwash thickness (as measured by the first lithologic contact) 67 cm shown by blue arrows.

Figure B.4

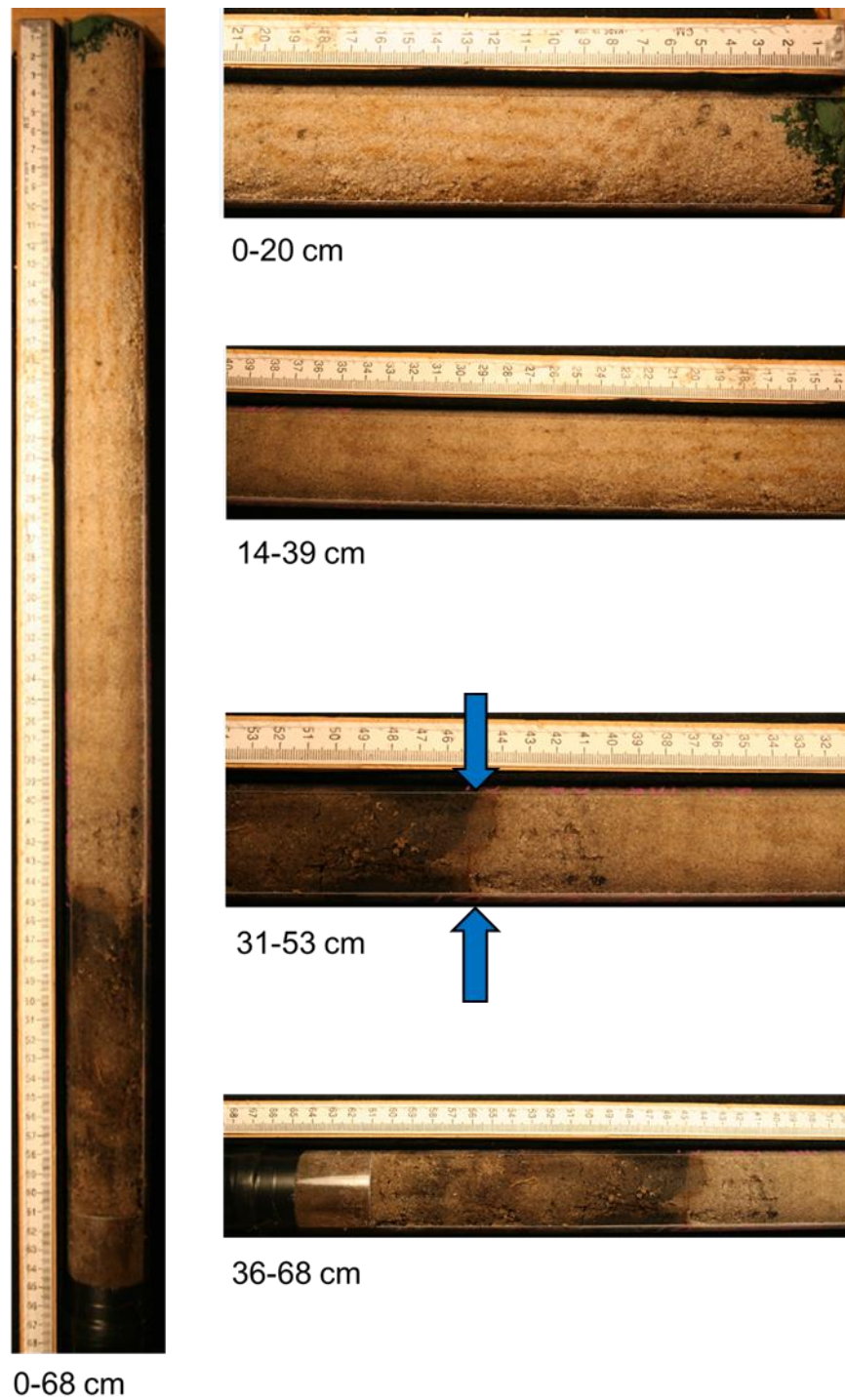


Figure B.4. Core BH-105-5 (150 m from the shoreline). Overwash thickness (as measured by the first lithologic contact) 43 cm shown by blue arrows.

Figure B.5

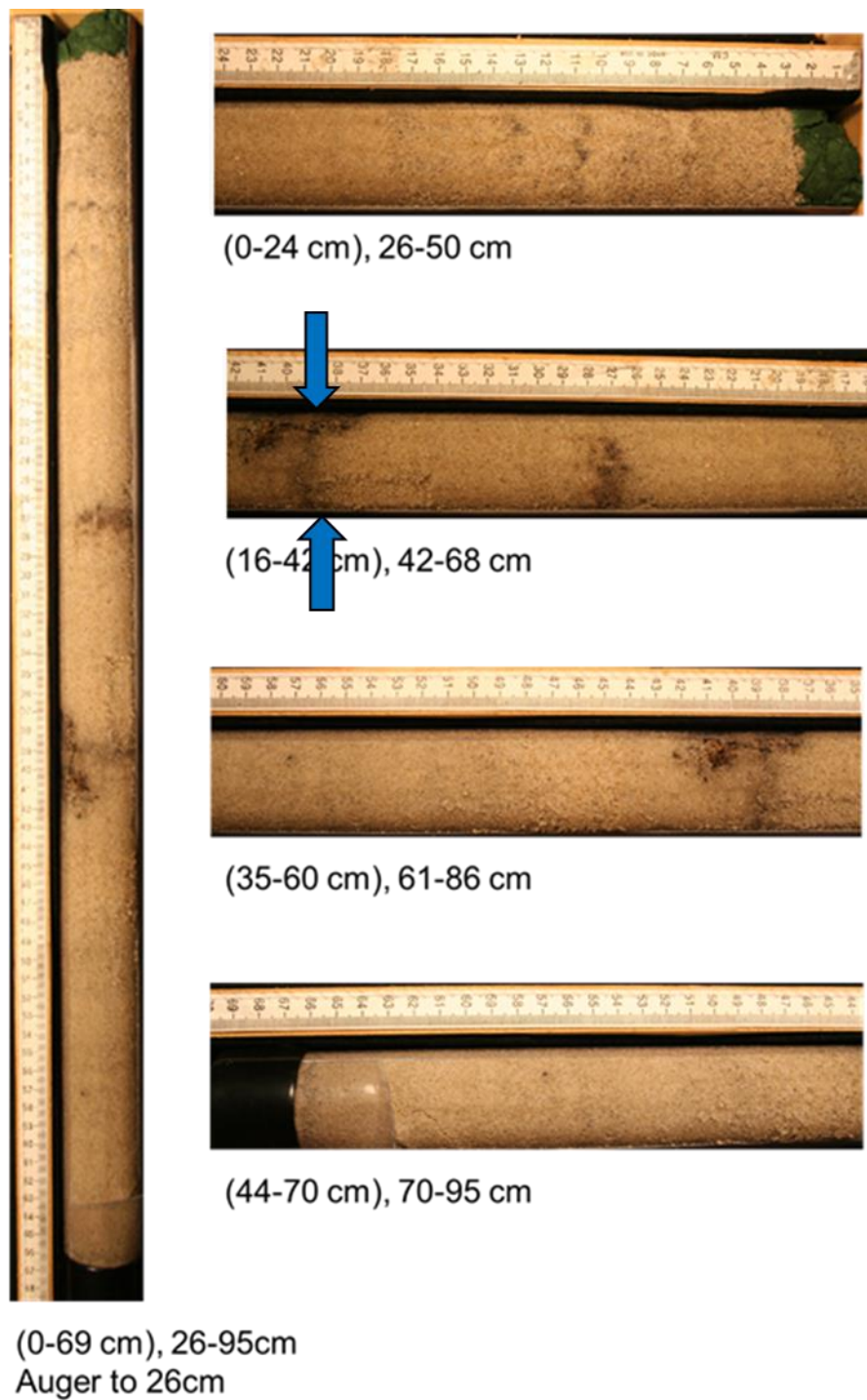


Figure B.5. Core BH-123-2-2 (90 m from the shoreline). Overwash thickness (as measured by the first lithologic contact) 65 cm shown by blue arrows.

Figure B.6

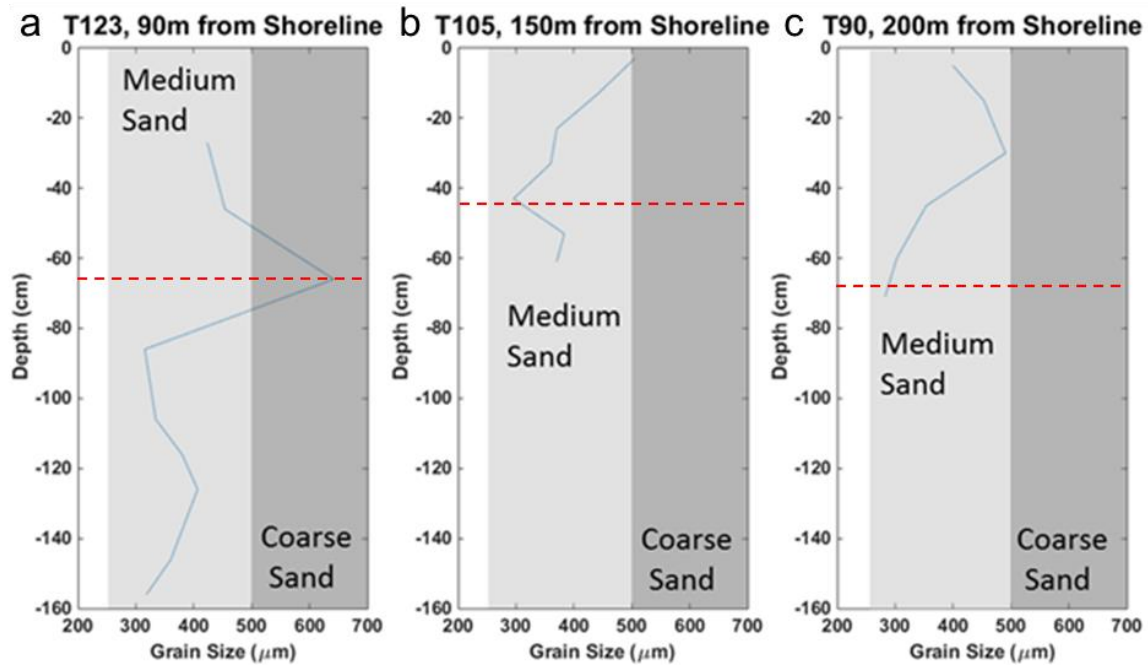


Figure B.6. Results of grain size analysis conducted using a Beckman Coulter LS 3 Series particle size analyzer. Samples were analyzed at 15 cm intervals from three cores located at different distances from the shoreline. Grain size is categorized using the Wentworth Scale. Overwash thickness as identified visually is depicted as red dashed lines at (a) Core 123-2-2 (Figure B.5) 65cm, (b) Core 105-5 (Figure B.4) 43cm and (c) Core 90-7 (Figure B.3) 67cm.

## REFERENCES

- Blake, E. S., Kimberlain, T. B., Berg, R. J., Cangialosi, J. P., & Beven II, J. L. (2013). Tropical Cyclone Report: Hurricane Sandy. *National Hurricane Center*, 12, 1-10.
- Carruthers, E. A., Lane, D. P., Evans, R. L., Donnelly, J. P., & Ashton, A. D. (2013). Quantifying overwash flux in barrier systems: An example from Martha's Vineyard, Massachusetts, USA. *Marine Geology*, 343, 15-28, doi:10.1016/j.margeo.2013.05.013.
- Cohn, N., Ruggiero, P., Ortiz, J., & Walstra, D. J. (2014). Investigating the role of complex sandbar morphology on nearshore hydrodynamics. *Journal of Coastal Research*, SI(70), 53-58, doi: 10.2112/SI65-010.1.
- Criss, R. E., & Shock, E. L. (2001). Flood enhancement through flood control. *Geology*, 29(10), 875-878, doi: 10.1130/0091-7613(2001)029<0875:FETFC>2.0.CO;2.
- Donnelly, C., Kraus, N., & Larson, M. (2006). State of knowledge on measurement and modeling of coastal overwash. *Journal of Coastal Research*, 22(4), 965-991, doi:10.2112/04-0431.1.
- Donnelly, C., & Sallenger, A. H. (2007). Characterization and modeling of washover fans. *Proceedings of Coastal Sediments' 07*, 2061-2073, doi: 10.1061/40926(239)162.
- Donnelly, C., Hanson, H., & Larson, M. (2009). A numerical model of coastal overwash. *Proceedings of the ICE-Maritime Engineering*, 162(3), 105-114, doi: 10.1680/maen.2009.162.3.105.
- Duran-Vinent, O., & Moore, L. J. (2015). Barrier island bistability induced by biophysical interactions. *Nature Climate Change*, 5(2), 158-162, doi: 10.1038/NCLIMATE2474.
- Emanuel, K. A. (2013). Downscaling CMIP5 climate models shows increased tropical cyclone activity over the 21st century. *Proceedings of the National Academy of Sciences*, 110(30), 12219-12224, doi: 10.1073/pnas.1301293110.
- FitzGerald, D. M., Fenster, M. S., Argow, B. A., & Buynevich, I. V. (2008). Coastal impacts due to sea-level rise. *Annu. Rev. Earth Planet. Sci.*, 36, 601-647.
- Hall, M. J., & Halsey, S. D. (1991). Comparison of Overwash Penetration from Hurricane Hugo and Pre-Storm Erosion Rates for Myrtle Beach and North Myrtle Beach, South Carolina, USA. *Journal of Coastal Research*, 229-235.
- Hodgson, M. E., & Bresnahan, P. (2004). Accuracy of Airborne Lidar-Derived Elevation. *Photogrammetric Engineering & Remote Sensing*, 70(3), 331-339.
- Honey, M., & Krantz, D. (2007). Global trends in coastal tourism. *Washington DC: Center on Ecotourism and Sustainable Development*.

- Houser, C. (2013). Alongshore variation in the morphology of coastal dunes: Implications for storm response. *Geomorphology*, 199, 48-61, doi: 10.1016/j.geomorph.2012.10.035.
- Jackson, J. B., Kirby, M. X., Berger, W. H., Bjorndal, K. A., Botsford, L. W., Bourque, B. J., ... & Warner, R. R. (2001). Historical overfishing and the recent collapse of coastal ecosystems. *Science*, 293(5530), 629-637, doi: 10.1126/science.1059199.
- Jin, D., Ashton, A. D., & Hoagland, P. (2013). Optimal responses to shoreline changes: an integrated economic and geological model with application to curved coasts. *Natural Resource Modeling*, 26(4), 572-604, doi: 10.1111/nrm.12014.
- Knutson, T. R., McBride, J. L., Chan, J., Emanuel, K., Holland, G., Landsea, C., ... & Sugi, M. (2010). Tropical cyclones and climate change. *Nature Geoscience*, 3(3), 157-163. doi: 10.1038/ngeo779.
- Kopp, R. E., Horton, R. M., Little, C. M., Mitrovica, J. X., Oppenheimer, M., Rasmussen, D. J., ... & Tebaldi, C. (2014). Probabilistic 21st and 22nd century sea-level projections at a global network of tide-gauge sites. *Earth's Future*, 2(8), 383-406., doi: 10.1002/2014EF000239.
- Lazarus, E. D. (2014). Threshold effects of hazard mitigation in coastal human–environmental systems. *Earth Surface Dynamics*, 2(1), 35-45, doi:10.5194/esurf-2-35-2014.
- Lazarus, E. D., & Armstrong, S. (2015). Self-organized pattern formation in coastal barrier washover deposits. *Geology*, 43(4), 363-366, doi: 10.1130/G36329.1.
- Leatherman, S. P. (1983). Barrier dynamics and landward migration with Holocene sea-level rise. *Nature*, 301, 15-17, doi: 10.1038/301415a0.
- Lorenzo-Trueba, J., & Ashton, A. D. (2014). Rollover, drowning, and discontinuous retreat: Distinct modes of barrier response to sea-level rise arising from a simple morphodynamic model. *Journal of Geophysical Research: Earth Surface*, 119(4), 779-801, doi: 10.1002/2013JF002941.
- Magliocca, N. R., McNamara, D. E., & Murray, A. B. (2011). Long-term, large-scale morphodynamic effects of artificial dune construction along a barrier island coastline. *Journal of Coastal Research*, 27(5), 918-930, doi: 10.2112/jcoastres-d-10-00088.1.
- McCallum, B. E., Wicklein, S. M., Reiser, R. G., Busciolano, R., Morrison, J., Verdi, R. J., ... & Gotvald, A. J. (2013). *Monitoring storm tide and flooding from Hurricane Sandy along the Atlantic coast of the United States, October 2012* (No. 2013-1043, pp. 1-42). US Geological Survey.
- McNamara, D. E., & Keeler, A. (2013). A coupled physical and economic model of the response of coastal real estate to climate risk. *Nature Climate Change*, 3(6), 559-562, doi: 10.1038/NCLIMATE1826.

- McNamara, D. E., & Werner, B. T. (2008a). Coupled barrier island–resort model: 1. Emergent instabilities induced by strong human-landscape interactions. *Journal of Geophysical Research: Earth Surface* (2003–2012), 113(F1), doi: 10.1029/2007JF000840.
- McNamara, D. E., & Werner, B. T. (2008b). Coupled barrier island–resort model: 2. Tests and predictions along Ocean City and Assateague Island National Seashore, Maryland. *Journal of Geophysical Research: Earth Surface* (2003–2012), 113(F1), doi: 10.1029/2007JF000841.
- Miselis, J., Andrews, B., Ganju, N., Navoy, A., Nicholson, R., & Defne, Z. (2013) Mapping, Measuring, and Modeling to Understand Water-Quality Dynamics in Barnegat Bay-Little Egg Harbor Estuary, New Jersey. *Sound Waves*. 2013(2). Retrieved from <http://soundwaves.usgs.gov/2013/02/>.
- Morton, R. A., & Sallenger Jr, A. H. (2003). Morphological impacts of extreme storms on sandy beaches and barriers. *Journal of Coastal Research*, 560-573.
- National Oceanic and Atmospheric Administration. (2013). NOAA Water Level and Meteorological Data Report: Hurricane Sandy. Retrieved from [www.tidesandcurrents.noaa.gov/publications/Hurricane\\_Sandy\\_2012\\_Water\\_Level\\_and\\_Meteorological\\_Data\\_Report.pdf](http://www.tidesandcurrents.noaa.gov/publications/Hurricane_Sandy_2012_Water_Level_and_Meteorological_Data_Report.pdf)
- National Oceanic and Atmospheric Administration. (2015). NOAA Tides and Currents. Retrieved from <http://tidesandcurrents.noaa.gov/sltrends/sltrends.html/>.
- Nordstrom, K. F. (1994). Beaches and dunes of human-altered coasts. *Progress in Physical Geography*, 18(4), 497-516, doi: 10.1177/030913339401800402.
- Palmsten, M. L., & Holman, R. A. (2012). Infiltration and instability in dune erosion. *Journal of Geophysical Research: Oceans* (1978–2012), 116(C10), doi: 10.1029/2011JC007083.
- Plant, N. G., & Stockdon, H. F. (2012). Probabilistic prediction of barrier-island response to hurricanes. *Journal of Geophysical Research: Earth Surface* (2003–2012), 117(F3), doi: 10.1029/2011JF002326.
- Psuty, N. P. (2002). *Coastal hazard management: Lessons and future directions from New Jersey*. Rutgers University Press.
- Redfield, A. C., & Miller, A. R. (1955). *Water levels accompanying Atlantic Coast hurricanes* (No. R55 28). Woods Hole Oceanographic Institution MA.
- Roelvink, D., Reniers, A., van Dongeren, A. P., de Vries, J. V. T., McCall, R., & Lescinski, J. (2009). Modelling storm impacts on beaches, dunes and barrier islands. *Coastal Engineering*, 56(11), 1133-1152, doi: 10.1016/j.coastaleng.2009.08.006.

- Sallenger Jr, A. H. (2000). Storm impact scale for barrier islands. *Journal of Coastal Research*, 16(3), 890-895.
- Sallenger, A., Krabill, W., Swift, R., & Brock, J. (2001). Quantifying hurricane-induced coastal changes using topographic Lidar. *Proceedings Coastal Dynamics 2001 (ASCE)*, 1007-1016.
- Sallenger Jr, A. H., Krabill, W. B., Swift, R. N., Brock, J., List, J., Hansen, M., ... & Stockdon, H. (2003). Evaluation of airborne topographic Lidar for quantifying beach changes. *Journal of Coastal Research*, 125-133.
- Schoennagel, T., Veblen, T. T., & Romme, W. H. (2004). The interaction of fire, fuels, and climate across Rocky Mountain forests. *BioScience*, 54(7), 661-676, doi: 10.1641/0006-3568(2004)054[0661:TIOFFA]2.0.CO;2.
- Shaw, J., You, Y., Mohrig, D., & Kocurek, G. (2015). Tracking hurricane-generated storm surge with washover fan stratigraphy. *Geology*, 43(2), 127-130, doi: 10.1130/G36460.1.
- Sherwood, C. R., Long, J. W., Dickhudt, P. J., Dalyander, P. S., Thompson, D. M., & Plant, N. G. (2014). Inundation of a barrier island (Chandeleur Islands, Louisiana, USA) during a hurricane: Observed water-level gradients and modeled seaward sand transport. *Journal of Geophysical Research: Earth Surface*, 119(7), 1498-1515, doi: 10.1002/2013JF003069.
- Stockdon, H. F., Sallenger Jr, A. H., List, J. H., & Holman, R. A. (2002). Estimation of shoreline position and change using airborne topographic Lidar data. *Journal of Coastal Research*, 18(3), 502-513.
- Stockdon, H. F., Doran, K. S., & Sallenger Jr, A. H. (2009). Extraction of Lidar-based dune-crest elevations for use in examining the vulnerability of beaches to inundation during hurricanes. *Journal of Coastal Research*, SI(53), 59-65, doi: 10.2112/SI53-007.1.
- Stocker, T. F., Qin, D., Plattner, G. K., Tignor, M., Allen, S. K., Boschung, J., ... & Midgley, B. M. (2013). IPCC, 2013: Climate Change 2013: the Physical Science Basis. Contribution of Working Group I to the Fifth Assessment Report of the Intergovernmental Panel on Climate Change.
- Thieler, E., Himmelstoss, E. A., Zichichi, J. L., & Ergul, A. (2009). *The Digital Shoreline Analysis System(DSAS) Version 4. 0- An ArcGIS Extension for Calculating Shoreline Change*. U. S. Geological Survey.
- Titus, J. G., Park, R. A., Leatherman, S. P., Weggel, J. R., Greene, M. S., Mausel, P. W., ... & Yohe, G. (1991). Greenhouse effect and sea level rise: the cost of holding back the sea. *Coastal Management*, 19(2), 171-204, doi: 10.1080/08920759109362138.

- Urquhart, E. A., Hoffman, M. J., Murphy, R. R., & Zaitchik, B. F. (2013). Geospatial interpolation of MODIS-derived salinity and temperature in the Chesapeake Bay. *Remote Sensing of Environment*, 135, 167-177.
- Walters, D., Moore, L. J., Duran Vincent, O., Fagherazzi, S., & Mariotti, G. (2014). Interactions between barrier islands and backbarrier marshes affect island system response to sea level rise: Insights from a coupled model. *Journal of Geophysical Research: Earth Surface*, 119(9), 2013-2031, doi: 10.1002/2014JF003091.
- Werner, B. T., & McNamara, D. E. (2007). Dynamics of coupled human-landscape systems. *Geomorphology*, 91(3), 393-407, doi: 10.1016/j.geomorph.2007.04.020.
- White, S. A., & Wang, Y. (2003). Utilizing DEMs derived from LIDAR data to analyze morphologic change in the North Carolina coastline. *Remote sensing of environment*, 85(1), 39-47, doi: 10.1016/S0034-4257(02)00185-2.
- Williams, H. F. L. (2015). Contrasting styles of Hurricane Irene washover sedimentation on three east coast barrier islands: Cape Lookout, North Carolina; Assateague Island, Virginia; and Fire Island, New York. *Geomorphology*, 231, 182-192, doi: 10.1016/j.geomorph.2014.11.027.
- Wolinsky, M. A., & Murray, A. B. (2009). A unifying framework for shoreline migration: 2. Application to wave-dominated coasts. *Journal of Geophysical Research: Earth Surface* (2003–2012), 114(F1), doi: 10.1029/2007JF000856.
- Wright, C. W., Fredericks, X., Troche, R. J., Klipp, E. S., Kranenburg, C. J., & Nagle, D. B. (2014). *EAARL-B coastal topography: eastern New Jersey, Hurricane Sandy, 2012: first surface* (No. 767). US Geological Survey.
- Zhang, K. & Zheng Cui. (2007). *Airborne LiDAR Data Processing and Analysis Tools*. National Center for Airborne Laser Mapping, International Hurricane Research Center.
- Zhang, K., & Leatherman, S. (2011). Barrier island population along the US Atlantic and Gulf Coasts. *Journal of Coastal Research*, 27(2), 356-363, doi: 10.2112/JCOASTRES-D-10-00126.1.
- Zhang, K., Whitman, D., Leatherman, S., & Robertson, W. (2005). Quantification of beach changes caused by Hurricane Floyd along Florida's Atlantic coast using airborne laser surveys. *Journal of Coastal Research*, 123-134, doi: 10.2112/02057.1